Rabi oscillations in a cavity-quantum dot system

THESIS

submitted in partial fulfillment of the
requirements for the degree of

BACHELOR OF SCIENCE
in
PHYSICS

Author :	Steven Riedijk
Student ID :	1693042
Group :	Dirk Bouwmeester
Supervisor :	Wolfgang Löffler
	Henk Snijders
2^{nd} corrector :	Martina Huber

Leiden, The Netherlands, July 16, 2018

Rabi oscillations in a cavity-quantum dot system

Steven Riedijk

Huygens-Kamerlingh Onnes Laboratory, Leiden University
P.O. Box 9500, 2300 RA Leiden, The Netherlands

July 16, 2018

Abstract

Rabi oscillations between the excited state and the ground state of an exciton in a quantum dot can be used to coherently control the state of a two-level system. Manipulating the state of a two-level systems has applications in quantum computing and creating single photon sources. Rabi oscillations have been amply observed in atoms, free-space quantum dots, and ion traps. However, observing this phenomenon in cavity quantum electrodynamics has shown to be much more demanding. In this thesis we show that Rabi oscillations can also be observed in polarisation non-degenerate cavity-quantum dot systems.

Contents

Chapter 1

Introduction

A major breakthrough in applied quantum physics occurred in 1992 when David Deutsch and Richard Jozsa demonstrated that quantum algorithms can solve certain problems considerably faster than classical deterministic algorithms [1]. Two years later the mathematician Peter Shor showed that contemporary encryption could be decoded in polynomial time with the use of so-called quantum bits [2]. Since then the interest in quantum computing in particular has grown rapidly. Quantum computing requires the aforementioned quantum bits or qubits for short. A qubit is a two-level quantum system which, in contrast to classical bits, can be in a superposition of both possible states. A classical bit can either be on ($|1\rangle$) or off ($|0\rangle$), while a quantum bit can be in a superposition of both states.

Multiple quantum properties and systems have been investigated as possible qubits. These systems include for example the spin of an electron [3], optomechanical systems [4], nuclear magnetic resonance systems [5], the photon polarisation [6] and photons [7]. Although these systems have shown to be valid possible qubits, they could be hard to produce *en masse* for actual quantum networks. In this project we will focus on one certain prospect: a cavity-quantum dot system.

A quantum dot is a semiconductor solid-state complex that behaves in many ways like an atom. In chapter **3** the specifics of our sample will be discussed. Electronic states in quantum dots exhibit atomic features as entanglement [8], photon antibunching [9] and Rabi oscillations [10]. Electronic states in a quantum dot satisfy a few requirements for a quantum bit. Firstly a quantum dot can potentially be initialised and controlled without interfering with neighbouring quantum dots. Furthermore, the

Version of July 16, 2018– Created July 16, 2018 - 17:34

optical photons that are used to initialise and control the quantum dot are able to transmit information via, for example, their polarisation. However, a bare quantum dot does not fulfil all the specifications for a quantum network. A reliable quantum network requires near-deterministic interaction of a photon with a qubit.

To accomplish this efficient coupling of the photons to our quantum dot the quantum dot is placed in a microcavity. A cavity confines light in space. An introduction to cavity quantum electrodynamics will be treated in chapter **2**. The effect of a cavity on the interaction probability is most easily understood in the case of a simple Fabry-Pérot cavity. A photon trapped in a Fabry-Pérot cavity will bounce back and forth between the two mirrors, effectively increasing the interaction chance between the small (10 nm) quantum dot and the 930 nm light wave [11]

In the same chapter we will also derive that a strong coupling of the cavity to the quantum dot will lead to Rabi oscillations and how the Rabi frequency relates to the electric field in the cavity. Rabi oscillations describe the oscillatory behaviour of the state of a two-level system. The procedure to measure Rabi oscillations in a cavity-quantum dot system can be simply described in three steps:

1. Find an efficient and reliable single-photon source;
2. Reduce light from other light sources;
3. Measure the number of photons emitted from this source as a function of laser power.

In practice, ”finding a reliable single-photon source” has been quite difficult. Chapter **4** will explain how a cavity-quantum dot system was found that acts as an ”efficient and reliable single-photon source”. An improvement to the original setup to block cavity light will be shortly discussed in chapter **5**. Finally, in chapter **6** we again return to the theory of Rabi oscillations and show that control of the state of a cavity-quantum dot system has in fact been realised and how the observation of Rabi oscillations relates to the detuning between the cavity frequency and the quantum dot frequency.

Chapter 2

Cavity Quantum Electrodynamics

In this chapter the basic theory and concepts behind Rabi oscillations and cavity quantum electrodynamics (CQED) will be studied. Furthermore, we will theoretically explore Rabi oscillations in a cavity-quantum dot system using a simple quantum master equation and give the result obtained from a more complete quantum master equation. Finally, by discussing earlier work on Rabi oscillations in self-assembled quantum dots this thesis is placed within the wider scientific context.

2.1 Rabi oscillations

Rabi oscillations describe the oscillatory behaviour of the excited state probability amplitude in a two-level system (Figure 2.1a). The derivation of this effect in vacuum is described by numerous sources [12–14]. For a simple two-level system starting in the ground state without a cavity the evolution of the probability amplitude is given by:

$$P_e = \sin^2(\theta/2) \tag{2.1}$$

The argument of the sinusoidal function is given by the pulse area. The pulse area is defined as the electric field integrated over time i.e. [14]:

$$\theta = \left| \frac{\mu_{01}}{\hbar} \int_{-\tilde{t}/2}^{\tilde{t}/2} E(t)\, \mathrm{d}t \right|, \tag{2.2}$$

where μ_{01} is the transition dipole element of the transition between the two states, E the electric field strength, $\hbar$ the reduced Planck constant, and $\pm\tilde{t}/2$ indicates the duration of the pulse. Rabi oscillations are often plotted

against time giving, without decaying effects, a so-called Rabi frequency given by [11, 13, 14]:

$$\Omega_0 = \left| \frac{\mu_{01} E_0}{\hbar} \right| \tag{2.3}$$

In the Bloch sphere representation the state of a two-level system is shown as a unitary sphere where the "south pole" corresponds to a state completely in the $|1\rangle$ state and the "north pole" corresponds to a state in the $|0\rangle$-state (Figure 2.1b). A superposition of those states can be represented as a vector in a different direction. This is possible, because both the norm of an unit vector as the probability of a quantum mechanical state is equal to 1 and because both the unit vector as the two-level system can be described by just two parameters. The coefficients c_1 and c_2 describing the state of a two-level system (e.g. $|\Phi\rangle = c_1 |0\rangle + c_2 |1\rangle$) can be written in polar coefficients of the unit vector as [14]:

$$\begin{aligned} c_0 &= \sin \theta / 2 \\ c_1 &= e^{i\phi} \cos \theta / 2 \end{aligned} \tag{2.4}$$

In this representation the pulse area can be viewed as the angle of rotation around the y-axis. A π-pulse thus rotates the state $|0\rangle$ into the state $|1\rangle$, while a 2π-pulse rotates a system back to its original state. The parameter ϕ can be manipulated by applying two pulses with a certain phase difference between the pulses. The state of a two-level system can thus be controlled by applying a series of pulses. Remark that the system will emit a photon when its state changes from the excited state to the ground state.

2.2 Rabi oscillations in CQED systems

In this thesis we study Rabi oscillations in cavity systems. The quest for reliable single photon sources or quantum bits resolves around creating an efficient interaction between an optical two-level system and a two-level system. To achieve this efficient interaction, a two-level system is placed into a cavity, where the cavity acts as an optical resonator. The effect of the cavity can be viewed in the classical picture as creating a standing wave or as a photon bouncing back and forth between the two mirrors effectively increasing the chance of an interaction between the photon and the cavity. The probability of an interaction between the photon and the quantum dot thus increases [11].

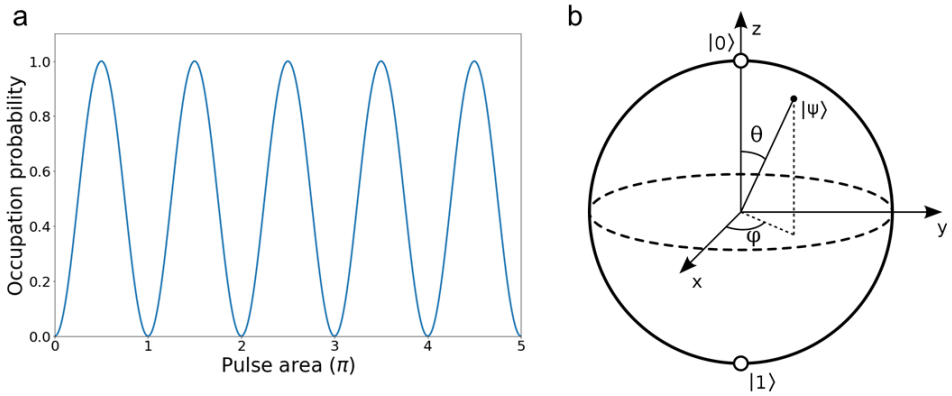

Figure 2.1 – **a** Simulated Rabi oscillations of the excited population in an ideal two-level system plotted against the applied pulse area. At $\theta = \pi$ the quantum dot is completely in the excited state, while at $\theta = 2\pi$ the quantum dot is back in its ground state. **b** The Bloch sphere. $-\hat{\mathbf{z}}$ and $\hat{\mathbf{z}}$ describe the states $|1\rangle$ and $|0\rangle$. Coherent superpositions of those states are given by unit vectors in different directions. The polar coordinates of this vector are given by equation 2.4.

However, deterministic interaction between an (artificial) atom and a photon is only realised in the case that :

$$C = \frac{g^2}{\kappa\gamma} \gg 1 \tag{2.5}$$

Here C is the cooperativity, κ is the intensity damping of the cavity, γ the dephasing rate of the quantum dot, and g the coupling constant between the cavity and the quantum dot [15]. An intuitive picture of a cavity and these constants is shown in figure 2.2.

Furthermore, by placing the quantum dot inside the cavity we can make use of the Purcell effect. The Purcell effect describes the change in the spontaneous emission rate of an atom or artificial atoms placed in a resonant or non-resonant cavity. The Purcell enhancement of the spontaneous emission rate for a dipole parallel with the cavity and on resonance with the cavity is given by [14, 16]:

$$F_p = \frac{3Q}{4\pi^2 V}\frac{\lambda^3}{n^3}, \tag{2.6}$$

with Q the quality factor, λ the wavelength of the light, V the modal volume, and n the refractive index. Considering the samples studied in this

Version of July 16, 2018– Created July 16, 2018 - 17:34

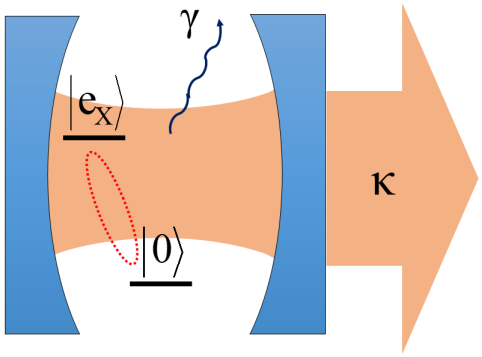

Figure 2.2 – Schematic of a cavity with an (artificial) atom. Cavity is indicated by two bend mirrors. κ describes the decay rate caused by photon loss from the mirrors and γ the decay rate induced by photon emitted into non light confining directions.

thesis with $n \approx 3.5$, $\lambda \approx 935$ nm, a Q-factor of approximately $2.0 \cdot 10^4$, and a modal volume V of 2.7 μm^3 [15], the cavities enhance the spontaneous emission rate with at most a factor 9. The cavities studied in this thesis thus enhance the spontaneous emission rate.

In contrast to free space, Rabi oscillations are much harder to detect in cavity-quantum dot systems. Here dephasing becomes important and the radiative recombination time is very fast, sometimes below a nanosecond. To properly describe the interaction between the cavity and a two-level system we will make use of the Jaynes-Cummings Hamiltonian. The Jaynes-Cummings Hamiltonian describes the interaction between a quantized mode of a cavity and a two-level system. The Jaynes-Cummings Hamiltonian is given by:

$$H_{JC} = \underbrace{\hbar\omega_c a^\dagger a}_{\text{Cavity term}} + \underbrace{\hbar\omega_{qd}\sigma^\dagger\sigma}_{\text{Quantum dot term}} + \underbrace{\hbar g(a\sigma^\dagger + a^\dagger\sigma)}_{\text{Cavity-quantum dot coupling}} , \tag{2.7}$$

(2.8)

where $a^\dagger$ and a are respectively the creation and annihilation operator which increase or decrease the number of photons in the combined cavity-quantum dot system. The quantum dot raising and lowering operators are given by $\sigma^\dagger$ and σ which increase or decrease the occupation of the quantum dot. ω_c and ω_{qd} correspond to the eigenfrequency of the cavity and the quantum dot, while g is the coupling constant between the quantum

dot and the cavity field which is equal to $\Omega_{cav}/2$. A more complete picture can be found in literature [11–13].

This Hamiltonian can be used to predict the behaviour of a two-level system in interaction with a cavity. To also correctly describe dephasing effects we will use a simple quantum master equation together with the interaction part of the aforementioned Jaynes-Cummings Hamiltonian. A quantum master equation describes the evolution of the density matrix. The diagonal elements of the density matrix are the probabilities, while the off-diagonal elements contain the correlations. The quantum master equation and the interaction part of the Jaynes-Cummings Hamiltonian are given by:

$$\begin{aligned} \frac{\mathrm{d}\hat{\rho}(t)}{\mathrm{d}t} &= -\frac{i}{\hbar}[H_{Int}, \hat{\rho}] \\ H_{int} &= \frac{\hbar}{2}\Omega_0(a\sigma^\dagger + a^\dagger\sigma) \end{aligned} \tag{2.9}$$

The bare quantum dot and cavity contributions to the Hamiltonian are discarded from this derivation for the sake of clarity as both terms give a zero contribution to the dynamics of the system. The two possible energy states are given by:

$$\begin{aligned} |1\rangle &= |e;0\rangle \\ |2\rangle &= |g;1\rangle \end{aligned}$$

This means that we do not account for energy loss in our system: the combined energy of the cavity and the quantum dot is the same in both states. Note that applying σ and $a^\dagger$ to $|2\rangle$ will result in a zero contribution as well as applying $\sigma^\dagger$ and a directly to $|1\rangle$. Following the thought process used by Gerry and Knight [13], we will make use of the definition of the density operator elements. i.e. $\langle i|\rho|j\rangle = \rho_{ij}$ and apply it element wise to equation 2.9. For the first matrix element ρ_{11} this is:

$$\langle 1|\frac{\mathrm{d}\rho(t)}{\mathrm{d}t}|1\rangle = \frac{i}{2}\Omega_0 \langle 1|((a\sigma^\dagger\rho + a^\dagger\sigma\rho - \rho a\sigma^\dagger + \rho a^\dagger\sigma)|1\rangle \tag{2.10}$$

Furthermore, we use that $\langle f|\hat{A}\hat{B}|g\rangle = \langle \hat{A}^\dagger f|\hat{B}|g\rangle$ and apply it multiple times to the above expression. Doing this gives us the following differential equation.

$$\frac{\mathrm{d}\rho_{11}(t)}{\mathrm{d}t} = \frac{i}{2}\Omega_0(\rho_{12} - \rho_{21}) \equiv \frac{i}{2}\Omega_0 A$$

Employing the same trick on the other 3 matrix elements yields a system of differential equations which we can express as just three equations because of the symmetry in ρ_{21} and ρ_{12}.

$$\frac{\mathrm{d}\rho_{11}(t)}{\mathrm{d}t} = i\frac{1}{2}\Omega_0(\rho_{12} - \rho_{21}) \equiv \frac{i}{2}\Omega_0 A \tag{2.11}$$

$$\frac{\mathrm{d}\rho_{22}(t)}{\mathrm{d}t} = i\frac{1}{2}\Omega_0(\rho_{21} - \rho_{12}) \equiv -\frac{i}{2}\Omega_0 A \tag{2.12}$$

$$\frac{\mathrm{d}\rho_{21}(t)}{\mathrm{d}t} = i\frac{1}{2}\Omega_0(\rho_{22} - \rho_{11}) = -\frac{\mathrm{d}\rho_{12}(t)}{\mathrm{d}t} \tag{2.13}$$

Because differentiation is a linear operation we can write this as an eigenvalue problem.

$$\frac{\mathrm{d}}{\mathrm{d}t}\begin{pmatrix}\rho_{11}\\ \rho_{22}\\ A\end{pmatrix} = \begin{pmatrix}0 & 0 & \frac{i}{2}\Omega_0\\ 0 & 0 & -\frac{i}{2}\Omega_0\\ i\Omega_0 & -i\Omega_0 & 0\end{pmatrix}\begin{pmatrix}\rho_{11}\\ \rho_{22}\\ A\end{pmatrix} \tag{2.14}$$

This system of equations gives us three eigenvalues: $\lambda_0 = 0$ and $\lambda_\pm = \pm i\Omega_0$. To solve this equation for the density matrix elements we have to find the eigenvectors and use the initial conditions. This calculation is trivial and hands us the following solution:

$$\rho(t) = c_1 e^{i\Omega_0 t}\begin{pmatrix}-\frac{1}{2}\\ \frac{1}{2}\\ 1\end{pmatrix} + c_2 e^{-i\Omega_0 t}\begin{pmatrix}\frac{1}{2}\\ -\frac{1}{2}\\ 1\end{pmatrix} + c_3\begin{pmatrix}1\\ 1\\ 0\end{pmatrix} \tag{2.15}$$

For the initial condition where the cavity-quantum dot system starts in the excited state (i.e. $|\Psi\rangle\,(t=0) = |1\rangle$) one has to solve equation 2.15 with $\rho(0) = (1\ 0\ 0)^T$. Working this out leaves us with the following equations for the density matrix elements:

$$\rho_{11} = \frac{1}{4}(e^{-i\Omega_0 t} + e^{i\Omega_0 t}) + \frac{1}{2} = \cos^2\frac{\Omega_0}{2}t \tag{2.16}$$

$$\rho_{22} = -\frac{1}{4}(e^{-i\Omega_0 t} + e^{i\Omega_0 t}) + \frac{1}{2} = \sin^2\frac{\Omega_0}{2}t \tag{2.17}$$

$$\rho_{12} - \rho_{21} = -\frac{1}{2}e^{-i\Omega_0 t} + \frac{1}{2}e^{i\Omega_0 t} = -i\sin(\Omega_0 t) \tag{2.18}$$

Version of July 16, 2018– Created July 16, 2018 - 17:34

Thus we find for a lossless system (or *closed* quantum system) the expected result. Note that the trace of the squared density matrix is 1 which indicates that this is a pure state [12].

One can also apply the same method to the more general Lindblad equation. The Lindblad equation describes an *open* quantum master system i.e. a system in contact with an environment. It is an expanded quantum master equation which also includes extra effects such as quantum dot dephasing and photon loss. Here we include only one additional term in the equation which describes the intensity damping of the cavity which gives us the following quantum master equation [11]:

$$\frac{\mathrm{d}\hat{\rho}(t)}{\mathrm{d}t} = -\frac{i}{\hbar}[H_{Int}, \hat{\rho}] - \kappa(a^\dagger a\rho + \rho a^\dagger a - 2a\rho a^\dagger), \tag{2.19}$$

with κ again the intensity damping of the cavity. The aforementioned calculation techniques can be used to solve this problem if we allow an additional energy state in which the quantum dot is in its ground state and the photon has leaked out of the cavity i.e. $|3\rangle = |g;0\rangle$. The calculation gives us three eigenvalues namely:

$$\lambda_0 = -\kappa \tag{2.20}$$

$$\lambda_\pm = -\kappa \pm \sqrt{\kappa^2 - \Omega_0^2} \tag{2.21}$$

These eigenvalues describe a decay the CQED system. For $\Omega_0 > \kappa$ the square root is imaginary and damped oscillations will be observed as expected . In the case of light damping, the system is expected to decay to a system with equal probability to be in the excited or ground state; since at high excitation powers, the stimulated emission and absorption rates become equal [13]. Strongly damped system, however, can decay to different excited state probabilities. [14]. Figure 2.3 shows a simulation of damped Rabi oscillations in a cavity.

2.3 Experimental observations of Rabi oscillations

A lot of earlier work already focused on Rabi oscillations in self-assembled quantum dots. In 2002 Zrenner et al. showed the existence of Rabi oscillations in a self-assembled InAs quantum dot surrounded by GaAs [17]. This was done by measuring the photocurrent induced by excited electrons. The experimental data can be found in figure 2.4b. Another group

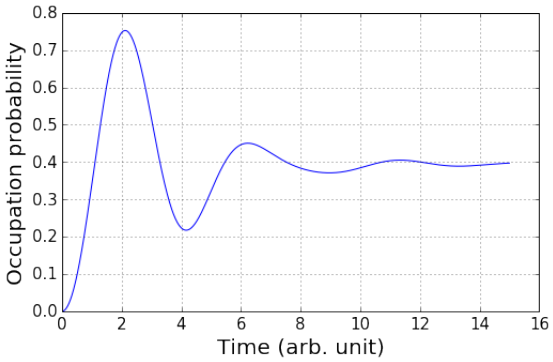

Figure 2.3 – Damped vacuum Rabi oscillations. Atom excited on resonance by a continuous laser. Figure made using the QuTiP python package with $\kappa = 0.1$, $\gamma = 0.01$, $g = 0.7$, $T = 2$, and $\omega_{qd} = \omega_{laser}$

in the early 2000s showed that Rabi oscillations can be observed in single quantum dots by looking at the change in transmission [10].

Rabi oscillations can also be observed directly in Hanbury Brown and Twiss measurements as demonstrated by Flagg et al. [18]. Hanbury Brown and Twiss experiments will be explained in more detail in chapter 6. A quantum dot excited with a high power continuous wave laser oscillates a few times before emission. This process is visible in the second-order correlation ($g^2(\tau)$) in continuous wave excitation.

In contrast to bare self-assembled quantum dots or in free-space atom experiments, Rabi oscillations have, as already mentioned, shown to be quite hard to measure in cavity-quantum dot systems. Recently Giesz et al. showed that Rabi oscillations are also visible in cavity-quantum dot systems and that population inversion could be achieved for only 3.8 photons [19]. The difference between their experiments and ours is that they only measured Rabi oscillations in reflection and did not couple the photons to a fiber, which makes the link to practical application a lot harder. A very interesting recent discovery regarding Rabi oscillations was done by Fischer et al. who demonstrated that in bare self-assembled quantum dots excited by a pulsed laser, multi-photon states are produced: a Gaussian excitation pulse leads to the production of two photons instead of single photons[20]. They observed that a π-pulse gives rise to antibunching ($g^2(0) < 1$) while excitation with a 2π-pulse leads to bunching ($g^2(0) > 1$). This can be explained by assuming a non-negligible pulse length and investigating the intra-pulse dynamics [21].

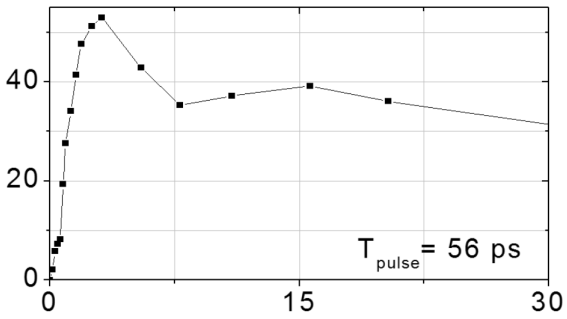

(a) Experimental observation of Rabi oscillations in a cavity-quantum dot system. Emission intensity in CCD counts times 100 versus the square root of the excitation power. Taken from [22]

.

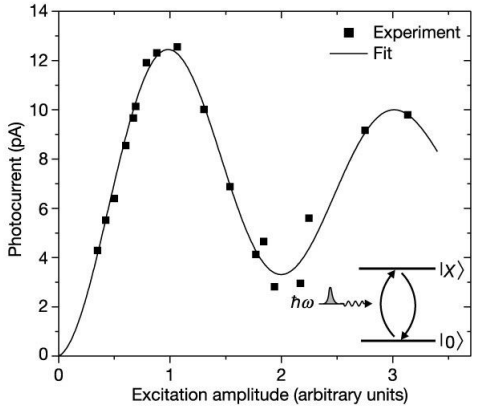

(b) Experimental observation of Rabi oscillations in free-space self-assembled quantum dots. Taken from [17].

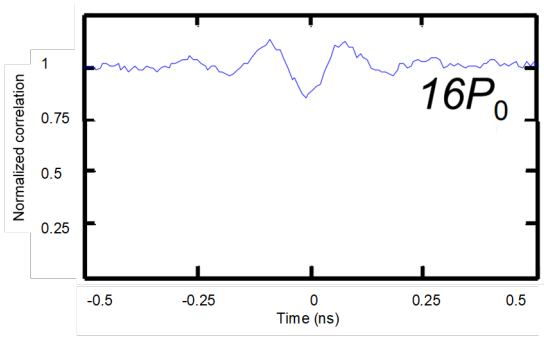

(c) Experimental observation of oscillations in the second-order correlation function for self-assembled quantum dots in a microcavity. Second-order correlation versus time delay. Figure taken from [23]. Font size labels rescaled using an image editor.

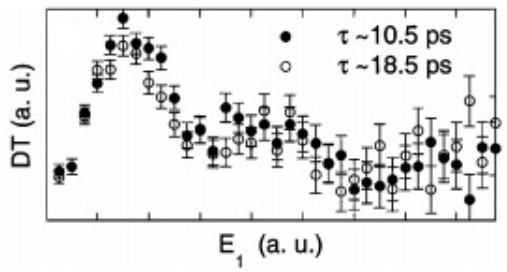

(d) Experimental observation of Rabi oscillations in a free-space self-assembled quantum dot. Change in transmission versus the strength of the electric field. Taken from [10].

Figure 2.4 – Experimental observations of Rabi oscillations in either cavity-quantum dot systems **(a,c)** or in bare solid-state quantum dots **(b,d)** in earlier works.

Chapter 3

Quantum dot and sample characteristics

In this thesis a quantum dot in a microcavity will be investigated for the study of Rabi oscillations. The cavity-quantum dot structures are grown and prepared at the UC Santa Barbara by Justin Norman and John Frey, respectively. The preparation of the microcavities and quantum dots can be found in earlier work [15, 24]. In this chapter the sample characteristics and the physics of the quantum dot will be discussed in more detail.

3.1 Sample characteristics

The cavity-quantum dot devices are placed on a array containing 42 different microcavities. The cavities confine light in the direction parallel to the incoming direction using Bragg mirrors, while light is confined using oxide apertures. All cavities have the same general design with an ellipse surrounded by three triangular shaped ”blades” as shown in figure 3.1b. Two parameters differ across the sample: the length of the semi-major axis and the length of the semi-minor axis of the micropillar. By varying the ellipticity of a cavity, the polarisation splitting of the fundamental cavity mode can be tuned. We will refer to the cavities by these two defining characteristics. For example, a device with a semi-minor axis of 30.0 μm and a semi-major axis of 32.5 μm will be referred to as 30.0-2.50, where 2.50 indicates the length difference to the semi-minor axis.

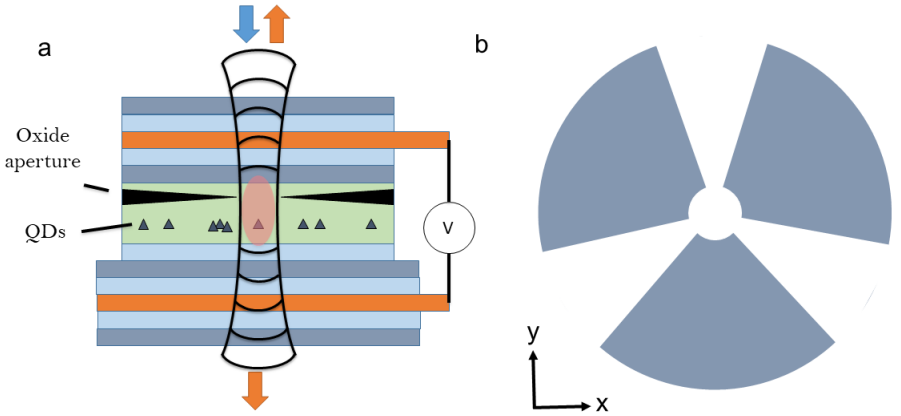

Figure 3.1 – **a** Schematic of the cross section of the microcavity. Bragg mirrors are represented by the light blue and dark blue sheets. The two large black triangles represent the oxide aperture which traps the light in the horizontal direction, while the small grey triangles represent quantum dots. The orange sheets indicate doped contact layers. **b** Schematic of the top of the microcavity. The ellipse is slightly longer in the y-direction than in the x-direction.

3.2 Quantum dot and band diagram

Atoms in solid-state materials cannot be seen as individual atoms. Electrons in solid-state materials interact with neighbouring electrons. This gives rise to a continuum of energy levels, resulting in bands of allowed energies. In the case of a semiconductor the Fermi energy is between two energy bands i.e. it is inside a (small) band gap. The band just below the Fermi energy is called the valence band, while the band above the Fermi energy is called the conductance band. The energy between the two bands is the band gap energy. If an electron is excited by, at least, the band gap energy, it will move from the valence band to the conductance band. Photons with energies less than the band gap will not be absorbed [25].

To create solid-state quantum dots the fact is used that different semiconductors have different band gap energies. In our case the quantum dot consists of small patches of Indium Arsenide (InAs) completely surrounded by Gallium Arsenide (GaAs). At 0 Kelvin, the semiconductor InAs has a band gap of 0.43 eV, while GaAs has a band gap of 1.52 eV [26]. This energy difference creates a de facto three-dimensional potential hole, the quantum dot. The flat band diagram shown in 3.2a shows this for a zero electric field. Using elementary quantum mechanics it can be shown that this confines the wave function of a charge carrier (i.e. elec-

tron or hole) in all dimensions and creates discrete energy levels. An electron in the conductance band can bind with a charged hole in the valence band [27]. Such a quasi-particle is called an exciton: a conductance band electron bound to a valence band hole. As mentioned in the introduction these excitons can exhibit atomic features as entanglement [8], photon antibunching [9] and Rabi oscillations [10]. Via spontaneous emission this system will re-emit a photon with the band gap energy and thus returns to the ground state of the two-level system.

The energy difference between the excited and the ground state of the two-level system is the energy difference between the highest energy state in the valence band and the lowest energy state in the conductance band. When an electric field is applied to the band diagram, the perturbation changes the potential and different energy states arise. That is, the lowest energy state in the conductance band lowers, while the highest energy state in the valence band increases. This effect is called the quantum-confined Stark effect [28]. The energy difference of the two-level system thus decreases. This is illustrated in figure 3.2b.

As could be seen in figure 3.1a the quantum dot is placed in the intrinsic reqion of a p-i-n junction, this creates a static electric field from the n-doped to the p-doped areas (see figure 3.3a). By applying a voltage to the sample, the potential difference between the n-doped and p-doped areas decreases. Therefore, the electric field created by this potential difference weakens. The band diagram thus converges to that of a flat band diagram [16]. Therefore, a larger bias creates a larger energy difference in our two-level system, using this the quantum dot can be tuned in resonance with the cavity.

3.3 Polarisation non-degenerate CQED

The exciton in our system cannot be simply described as a two-level system. The excited state is split into two non-degenerate polarisation energy states with linear eigenpolarizations $|X\rangle$ and $|Y\rangle$. Hence the exciton has in fact three possible states: $|g\rangle$, $|e_X\rangle$ and $|e_Y\rangle$. The Jaynes-Cummings Hamiltonian introduced in chapter 2 should thus be split into a X-term and a Y-term i.e.

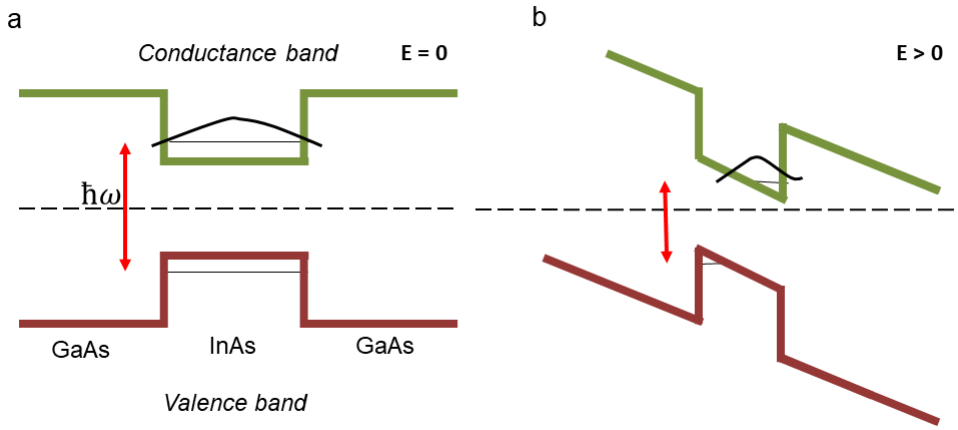

Figure 3.2 – Band diagram of the InAs/GaAs self-assembled quantum dot showing the quantum-confined Stark effect. **a** No electric field. **b** Electric field. The red arrow indicates the size of the energy gap of the two-level system. An electric field perturbation lowers the lowest energy state in the conductance band and increases the highest energy state in the valence band. Black lines indicate these energy states, while the black curve is a sketch of the wavefunction of a charge carrier in the potential hole.The vertical axis indicate energy, while the horizontal axis represents a spatial dimension. The dotted line shows the Fermi energy.

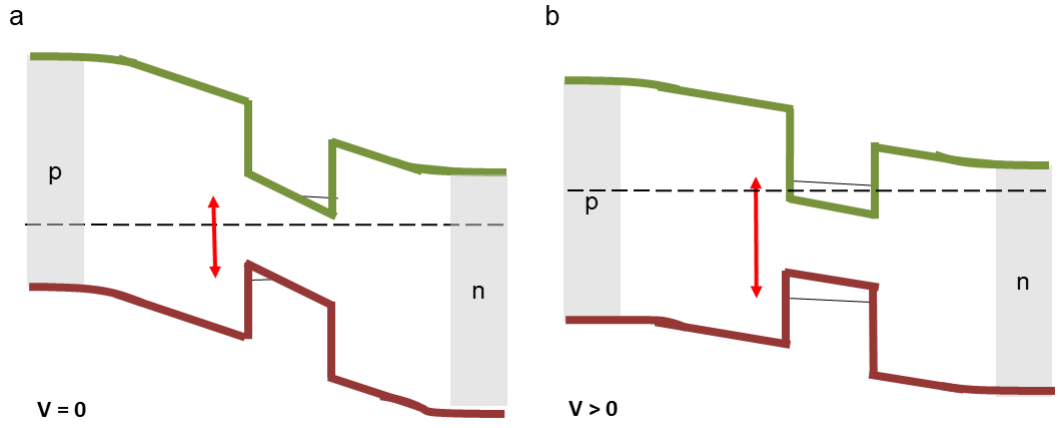

Figure 3.3 – Band diagram of the InAs/GaAs self-assembled quantum dot embedded in a p-n junction. **a** No bias applied. **b** Bias applied.

$$H_{JC} = \underbrace{\hbar\omega_c(a_X^\dagger a_X + a_Y^\dagger a_Y)}_{\text{Cavity term}} + \underbrace{\hbar\omega_{QD}(\sigma_X^\dagger\sigma_X + \sigma_Y^\dagger\sigma_Y)}_{\text{Quantum dot term}} + \tag{3.1}$$

$$\underbrace{\hbar g(a_X\sigma_X^\dagger + a_X^\dagger\sigma_X + a_Y\sigma_Y^\dagger + a_Y^\dagger\sigma_Y)}_{\text{Cavity-quantum dot coupling}} \tag{3.2}$$

Moreover, another complication in our system is that the cavity itself is also polarisation non-degenerate with eigenmodes $|H\rangle$ and $|V\rangle$. The orientation of the polarisation of the optical eigenmodes is not necessarily equal to the two dipoles of the quantum dot. We call the angle between these two modes the quantum dot angle [29]. A representation of this angle can be seen in figure 3.4b. The eigenstates of the exciton can be written in the cavity basis as:

$$|X\rangle = \cos(\theta_{QD})\,|H\rangle - \sin(\theta_{QD})\,|V\rangle \tag{3.3}$$

$$|Y\rangle = \sin(\theta_{QD})\,|H\rangle + \cos(\theta_{QD})\,|V\rangle \tag{3.4}$$

Thus, a $|H\rangle$ excited quantum dot will emit light in a superposition of $|X\rangle$ and $|Y\rangle$ polarised light and thus also emit photons with a vertical component (as long as θ_{QD} is not a multiple of π). The difference between the eigenpolarisations of the quantum dot and the cavity is used to only measure light from the quantum dot by extinguishing the cavity mode.

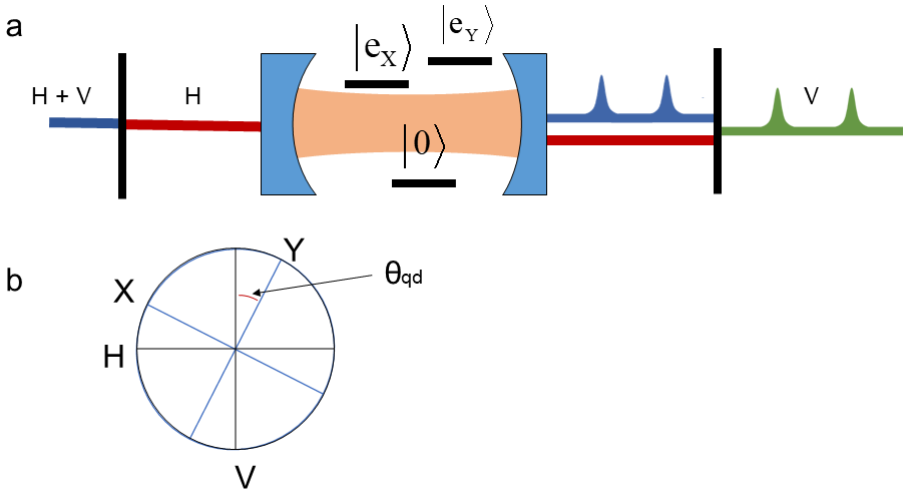

Figure 3.4 – **a** Schematic of a method to block the cavity mode. Blue lines indicate light which is both $|H\rangle$ and $|V\rangle$ polarised, red lines indicate $|H\rangle$ polarised light, green lines $|Y\rangle$ polarised light and the black vertical lines two polarisers. The cavity-quantum dot is represented as two mirrors with a two-level system in between **b** A visualisation of the angle between the cavity modes and the quantum dot modes.

Chapter 4

Device Characterisation

In this chapter first the general setup to characterise the introduced cavity-quantum dot samples will be introduced. The following sections will treat one particular type of measurement to find a cavity-quantum dot device suitable to measure Rabi oscillations. We discuss how a quantum dot is found, how the relevant parameters were calculated and how the single photon purity of a quantum dot is measured. Every section will discuss the used method and results and, if needed, introduce a little bit of theory to understand that particular type of measurement. Results will be given either only for device 31.0-2.00 or for a number of microcavities to give a bit of intuition and understanding for the difference between devices. Device 31.0-2.00 is the device for which eventually Rabi oscillations were clearly observed. All measured microcavities treated in this thesis are on array 19 or array 20 of sample 160511AP1-27nm.

4.1 Experimental setup

The relevant parts to the experimental setup are shown in figure 4.1.
The micro-cavity quantum dot structure is placed into a cryostat at 5 Kelvin to reduce the thermal fluctuations.

In our experiments either a continuous wave (CW) laser or a pulsed laser source is used. These lasers are connected via optical fibers to the main part of the setup. The laser is via the *Exit* fiber connected to either a Fabry-Pérot interferometer or a spectrometer. The laser power is controlled via an orthogonal polariser and a computer-controlled half wave plate. The two computer-controlled wave plates before the objective are used to con-

trol the polarisation of the incoming light. The transmitted laser light is blocked via two computer-controlled wave plates and a polarizer. The transmitted quantum dot photons are then detected using single photon detectors. In the shown setup a non-polarising beam splitter is shown as well as a second photon detector. This part of the setup will be explained in more detail in section 4.4.

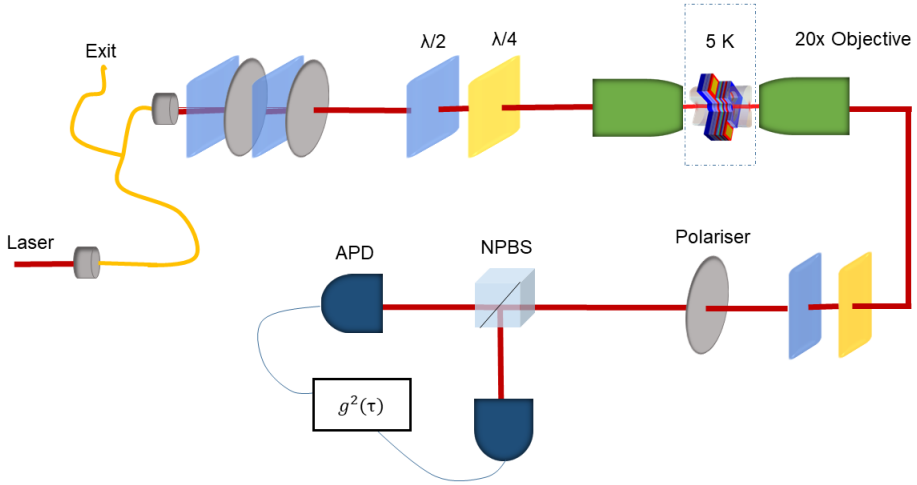

Figure 4.1 – Sketch of the experimental setup. $\lambda/2$ and $\lambda/4$ indicate half wave plates and quarter wave plates, respectively. NBPS is an acronym for non-polarising beam splitter, while APD stands for avalanche photodiode. The used detection scheme with two APDs and a non-polarising beam splitter is called a Hanbury-Brown-Twiss setup and will be explained in more detail in section 4.4.

4.2 Voltage scans

After the continuous wave laser is put on resonance with the cavity, we characterise a device by measuring the photon count while changing the voltage bias from 0.7 to 1.2 Volt. As shown in chapter 3 the band gap (and resonant frequency) of an InAs/GaAs quantum dot increases linearly with the applied voltage bias over the sample. By changing the voltage a quantum dot is tuned in resonance with the cavity. In total 47 microcavities were scanned for the existence of quantum dots. A subset of these voltage scans can be seen in figure 4.2. The broad horizontal high-intensity line indicates the fundamental mode of the cavity while the blue troughs indicate the presence of quantum dots. In general, a sharp low intensity line indicates a good quantum dot. This subset shows that there is an

abundance of quantum dots in our samples. Eventually, the device depicted in 4.2a was used to measure Rabi oscillations as it contained a very good and clean single-photon source. The quantum dot is indicated by a red arrow. The quantum dot was sufficiently spaced from other quantum dots and showed single photon emission under continuous wave excitation and pulsed laser excitation.

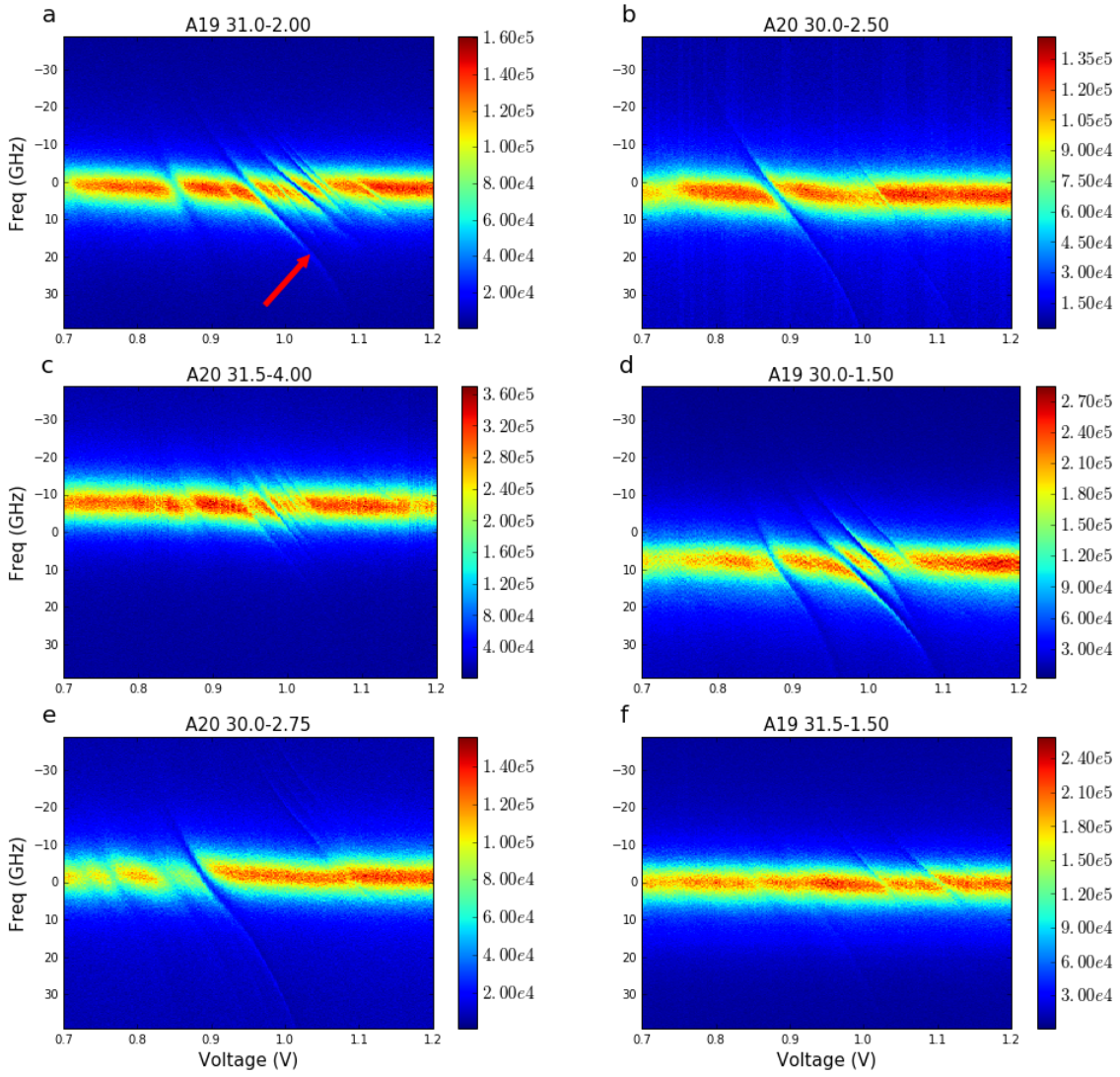

Figure 4.2 – The colour plots show $I(f, V)$ for six cavity-quantum dot systems. Data obtained by recording the transmitted photon counts, while scanning the laser (2 s) for each bias voltage (2 mV). Measured quantum dot in device 31.0-2.00 annotated by the red arrow.

To understand why a quantum dot decreases the intensity in transmission, we now investigate individual transmission and reflection spectra. The setup for a reflection measurement can be seen in figure 4.3. As shown in figure 4.4 most laser light is reflected off the cavity, and only a part enters the cavity. Note that only the part that actually enters the cavity will be able to interact with the quantum dot. If the quantum dot is excited, it will re-emit light, neglecting emission in other directions, in either the transmission or the reflection direction both with an amplitude given by:

$$t + r^2 t + r^4 t + \cdots = t \sum_{n=0}^{n=\infty} r^{2n} = \frac{t}{1 - r^2}, \tag{4.1}$$

with t the transmission coefficient and r the reflection coefficient of the Bragg mirrors. In contrast to the quantum dot emission, the incoming laser light is originally directed to the transmission axis. For the incoming beam to be seen in reflection an additional reflection is thus required i.e. the probability amplitude of the light beam in the cavity to be transmitted is given by $\frac{t}{1-r^2}$, while the probability amplitude to be reflected is given by $r \cdot \frac{t}{1-r^2}$. A quantum dot thus increases the luminosity in reflection, because in contrast to the original beam it has an equal chance to emit photons in reflection and transmission.

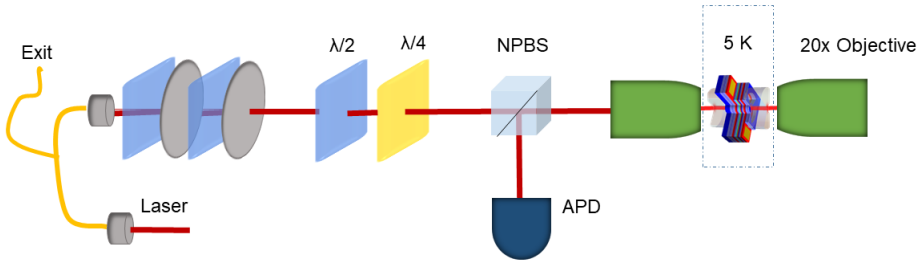

Figure 4.3 – Schematic of the setup used to measure the system in reflection.

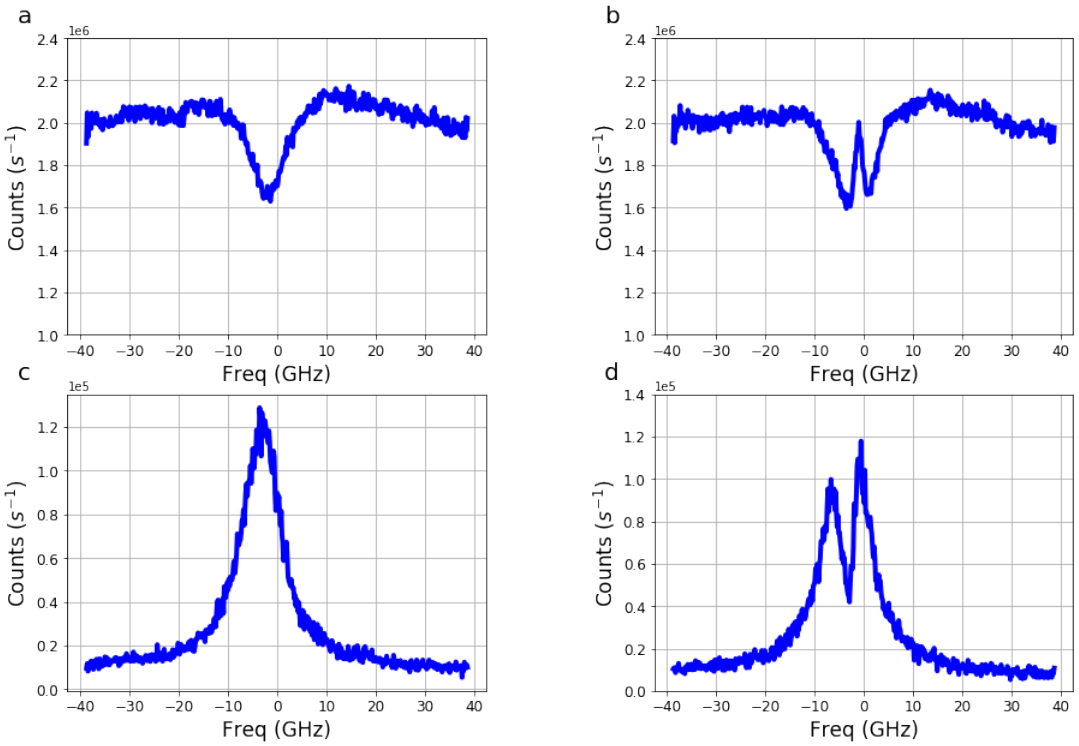

Figure 4.4 – Photon count versus frequency. Reflection **(a,b)** and transmission **(c,d)** spectra for the bare cavity **(a,c)** and for the case that a single quantum dot is tuned to be resonant with the cavity frequency **(b,d)**.

Version of July 16, 2018– Created July 16, 2018 - 17:34

4.3 Polarisation scans

A lot of the parameters describing the cavity-quantum dot system can be directly obtained from the transmitted signal. For excitation by a weak classical laser the transmission can be described with a semi-classical model. In the semi-classical view the transmission through a cavity-quantum dot system can be described as [30]:

$$t = \eta_{out} \frac{1}{1 - i\Delta + \frac{2C}{1 - i\Delta'}}, \tag{4.2}$$

with η_{out} as the output coupling efficiency, $\Delta = 2(\omega - \omega_c)/\kappa$ is the detuning between the laser frequency and the cavity frequency, C the cooperativity, $\Delta' = (\omega - \omega_{QD})/\gamma$ the detuning between the laser frequency and the quantum dot frequency.

Due to the polarisation non-degeneracy of our sample Δ and Δ' are different for different polarisations. (The full semi-classical transmission for a polarisation non-degenerate system can be found in [29]). This means that we cannot obtain our system parameters from a single frequency vs. intensity measurement. A complete picture also needs the quantum dot angle θ_{qd}, Δ and Δ' for both polarisation modes, and the intensity damping of the cavity κ for both polarisations.

This information can be taken from a scan over multiple incoming polarisations at a certain voltage. We measure this data by turning the first half wave plate in the set-up from 0 to 100 degrees and measure $I(f)$ for every angle. This will give us a three-dimensional data set with the number of counts, the polarisation angle and the frequency. In figure 4.5 six polarisation scans are shown. We can see that some devices are almost polarisation degenerate (4.5b) while others show a clear non-degeneracy (4.5d). The same can be observed for the polarisation degeneracy of the quantum dots (the blue lines in this figure). Note the quantum dot in figure 4.5e which is almost polarisation degenerate. Figure 4.5c also gives a nice illustration of the quantum dot angle: the polarisation modes of the quantum dot are clearly different from those of the cavity.

This data is fitted with a fitting program made by Henk Snijders. This is shown for device 31.0-2.00 in figure 4.6. It shows that the fitting procedure also works if there are a large number of quantum dots close together. The result of the other quantum dots is that the cavity signal looks lower and

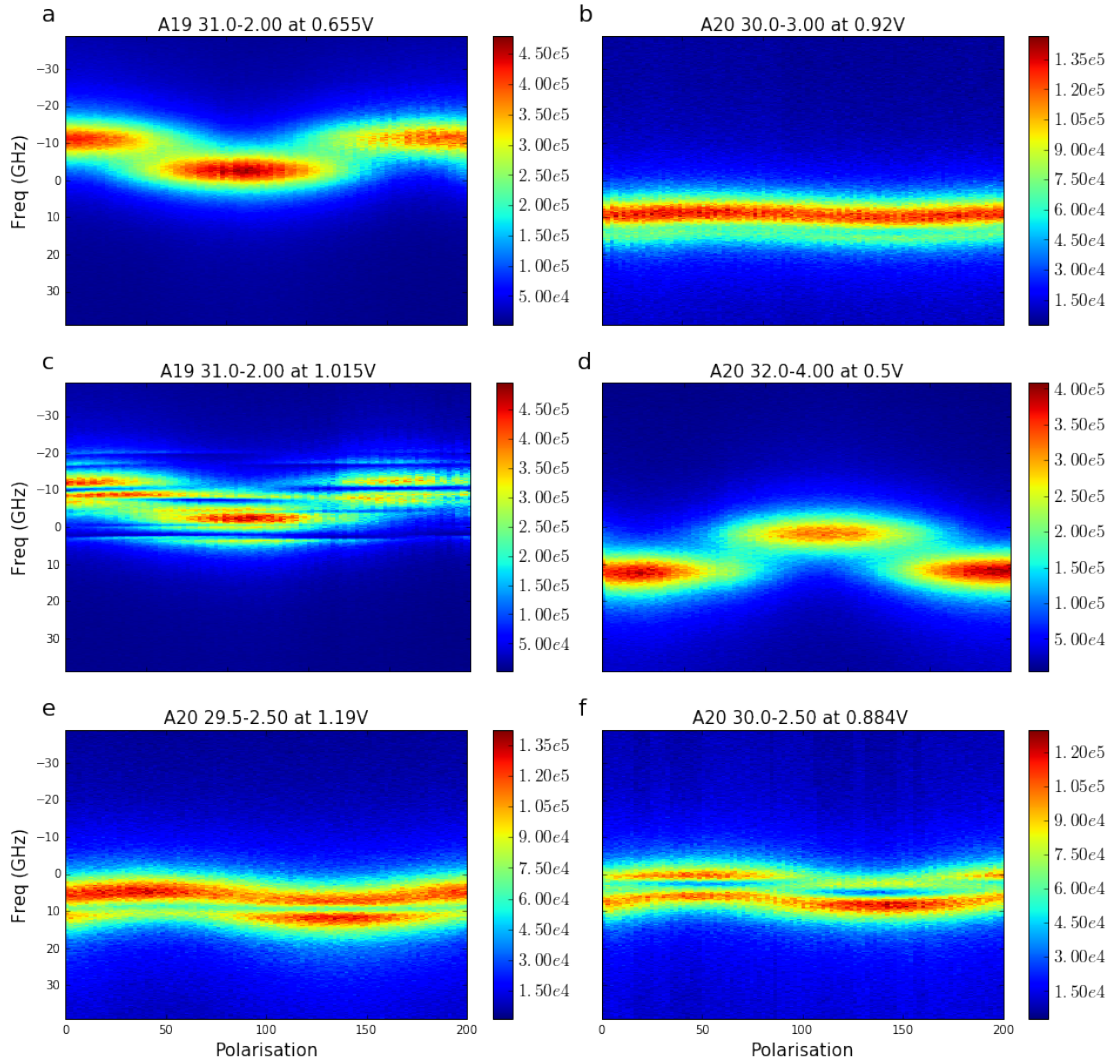

Figure 4.5 – The depicted colour plots show $I(f,\theta)$. The six polarisation scans for five different cavity-quantum dot devices show different levels of polarisation degeneracy. Data obtained by measuring the transmitted photon count in steps of 1 degree with a measurement time of 2 seconds under constant bias.

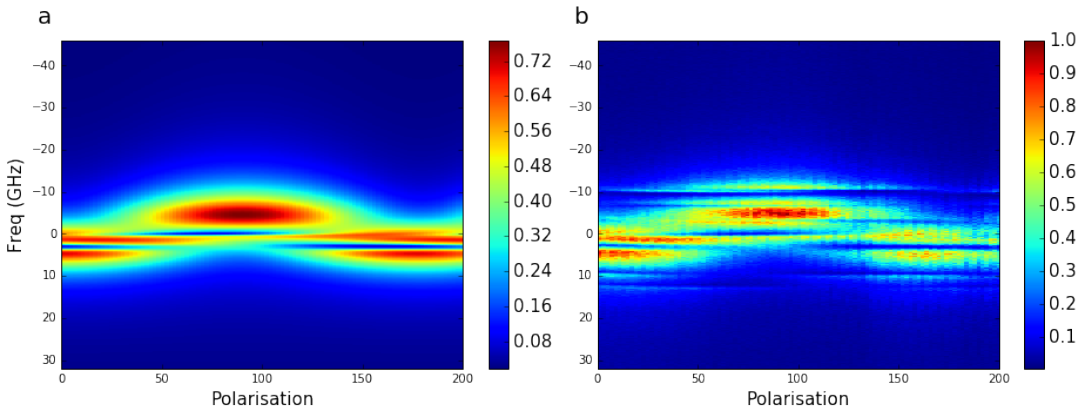

Figure 4.6 – **b** Colour plot shows the (normalised) raw data of the polarisation scan of device 31.0-2.00. **a** depicts the polarisation scan of device 31.0-2.00 fitted to the semi-classical model. The used parameters can be found in table 4.1.

Parameter	Value	Parameter	Value
κ_x	$52.64 \pm 5.35 \quad ns^{-1}$	κ_y	$65.55 \pm 6.59 \quad ns^{-1}$
γ	$1.49 \pm 0.90 \quad ns^{-1}$	g	$10.14 \pm 1.02 \quad ns^{-1}$
Δf_{qd}	$2.98 \pm 0.21 \quad ns^{-1}$	Δf_{cav}	$6.73 \pm 0.48 \quad ns^{-1}$
θ_{qd}	$-18.74 \pm 5.59 \quad (^\circ)$	η_{out}	0.76

Table 4.1 – Parameters used to fit the polarisation scan of device 31.0-2.00 to the semi-classical model.

the coupling constant, for example, will be slightly underestimated. The fitted data can be found in table 4.1.

4.3.1 Transition dipole moment of the quantum dot

To get an estimate for the order of magnitude of the Rabi frequency that will be measured in our setup, the value of the transition dipole moment μ_{01} in our system has to be known. An estimate of this value can be found with the fitted decay rate γ [see table 4.1]. In CQED the decay rate γ is given by [11]:

$$\gamma = \frac{\mu_{01}^2 \omega^3}{6\pi\epsilon_0 \hbar c^3}, \tag{4.3}$$

where ω is the angular frequency of the light inside the cavity. Rewriting this gives us an estimate for μ_{01} i.e.

$$\mu_{01}^2 = \frac{6\pi\epsilon_0 \hbar c^3 \gamma}{\omega^3} \tag{4.4}$$

Furthermore, we use that the frequency of the fundamental mode of the cavity is given by $\lambda \approx 935$nm which means that the angular frequency of the light inside the cavity is given by $\omega = 2\pi\frac{c}{\lambda}$. This gives us a transition dipole moment of:

$$\mu_{01}^2 = \frac{3\epsilon_0\hbar\lambda^3\gamma}{4\pi^2} \Longrightarrow \mu_{01} = 3.1 \cdot 10^{-28} \quad \text{Cm} \tag{4.5}$$

Multiple sources have reported the transition dipole moment of self-assembled InAs/GaAs quantum dots which show a transition dipole moment, at room temperature, in the order of $\mu_{01} = 1 \cdot 10^{-28}$ Cm in systems without a cavity [31, 32]. This is in good agreement with the calculated value.

4.4 Quantum dot as a single photon source

In this section the purity of the single-photon sources will be discussed. As mentioned before, to measure Rabi oscillations the quantum dot should emit single photons under both continuous wave excitation as well as under pulsed laser excitation. This can be measured using a Hanbury Brown and Twiss setup. Emission of single photon light is indicated by a low second-order correlation, that is $g^2[0] < 1$.

4.4.1 Hanbury-Brown-Twiss Interferometry

The second-order correlation ($g^2(\tau)$) of the light emitted by the cavity-quantum dot system is determined using a Hanbury Brown and Twiss interferometer. An illustration of Hanbury Brown and Twiss interferometry can be found in figure 4.7. Using a beam splitter, the signal is split into two arms. The photon count of each path is detected with seperate photon detectors. The delay between a photon count in detector 1 and detector 2 is registered via a start/stop circuit board. Thus, we measure the delay time between events in both detectors. Via this measurement we can experimentally measure the second-order coherence function of the emitted light. For coherent light, the photon pair will either both go the same detector or to two different detectors. If both photons go to different detectors we measure a coincidence event. For anti-bunched light (i.e. single photons), at zero time delay only one detector is activated and we register no coincidence counts at zero time delay. However, because of detector timing jitter, counts will still be measured at a zero time delay even for a perfect single photon source. A longer lifetime of a quantum dot will result in a lower dip than a quantum dot with a shorter lifetime even though the same actual single photon purity is obtained.

Additionaly, the $g^2(\tau)$ (i.e. number of coincidence counts) for coherent light (or uncorrelated light) is normalised to 1. A $g^2(0) < 1$ thus means that for a zero time delay, less coincidence counts were measured.

4.4.2 Continuous wave second-order coherence

As can be observed in figure 4.8 the second-order coherence function of 30.0-2.75 shows good single photon behaviour under CW excitation as was required to measure Rabi oscillations. A second-order correlation of $g^2(0) = 0.08$ is measured for a CW excitation of 1.49 ± 0.13 nW before the

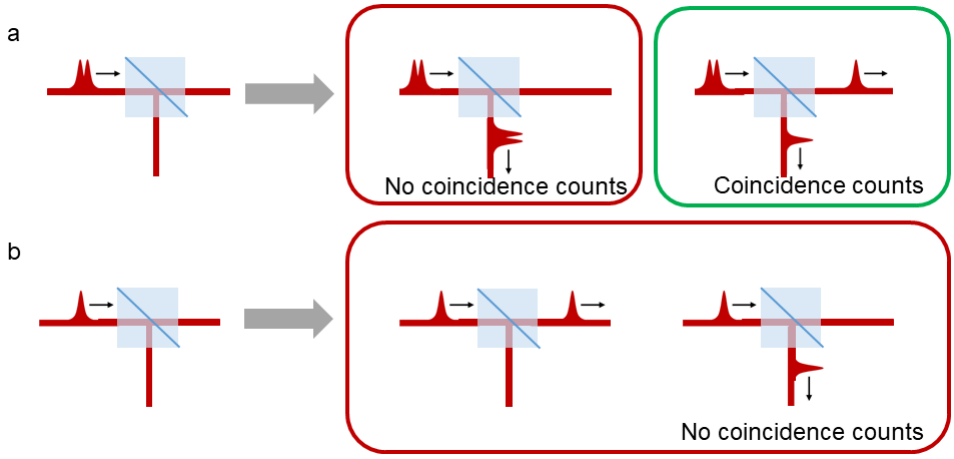

Figure 4.7 – Schematic of the Hanbury Brown and Twiss setup. Light either arrives in pairs (**a**) or as single photons (**b**). **a** If bunched light interacts with the beam splitter either both photons will leave via different paths and a coincidence count is measured for zero time delay or both photons leave via the same arm and no correlation is seen. **b** If anti-bunched light interacts with a beam splitter it will either be transmitted or deflected and only one detector "clicks" at a certain time. Ergo no correlation between the two detectors is measured for a zero time delay.

objective. We measured the second-order correlation for 10 different powers. Similar behaviour can be seen for device 31.0-2.00 in figure 4.9. The data tells us that both devices work as a single photon source with a high purity, which is required to measure Rabi oscillations with our method. In figure 4.10 the power versus second-order coherence relation is shown. This shows again that both devices work as single photon sources for a large range of powers under CW excitation.

4.4.3 Pulsed laser second-order coherence

However, to measure Rabi oscillations a CW laser cannot be used to excite the quantum dot. Furthermore, to measure Rabi oscillations the pulse duration has to be exactly defined. Stopping a CW laser with nanosecond or even picosecond precision is quite impossible. Therefore, instead of a CW laser, a pulsed laser is used to measure Rabi oscillations. A pulsed laser has a well defined pulse duration, such that a good temporal control can be achieved. Moreover, the low integrated intensity of a pulsed laser avoids charging of traps in the device.

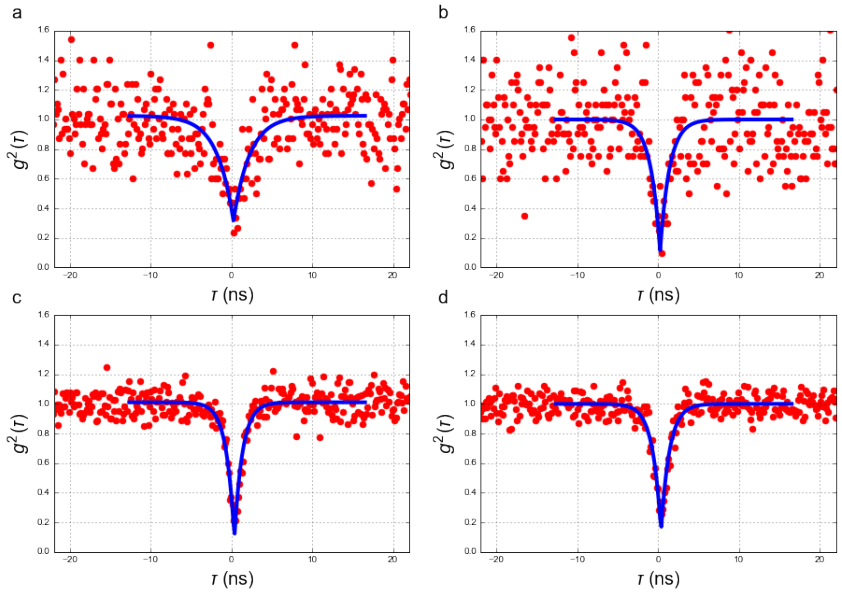

Figure 4.8 – Experimental second-order coherence measurements of cavity-quantum dot device 30.0-2.75 for different excitation powers. Blue lines represent a double exponential fit. **a-d** Second-order coherence $g^2(0) = 0.29$ (0.55 ± 0.05 nW), $g^2(0) = 0.11$ (0.88 ± 0.08 nW), $g^2(0) = 0.08$ (2.1 ± 0.19 nW), and $g^2(0) = 0.14$ (1.49 ± 0.13 nW), respectively.

For pulsed laser excitation we thus expect the second-order correlation function to consist of a row of peaks spaced 12.5 ns apart with roughly the same intensity. The second-order correlation at zero time delay is still expected to approach zero, as we expect the quantum dot to only emit single photons. This data is shown for device 31.0-2.00 (figure 4.11). Remark that the measured second-order coherence is higher than under CW excitation, which, considering that a laser pulse excites a larger frequency range than a CW laser, is to be expected. Furthermore, we observe that the system behaves as a better single photon source for lower powers. For device 30.0-2.75 a low single photon purity was observed. For this device, no Rabi oscillations were observed. In conclusion we see that device 31.0-2.00 works as a reliable and pure single photon source under both CW excitation as pulsed laser excitation and thus can be used to measure Rabi oscillations as postulated in chapter 2.

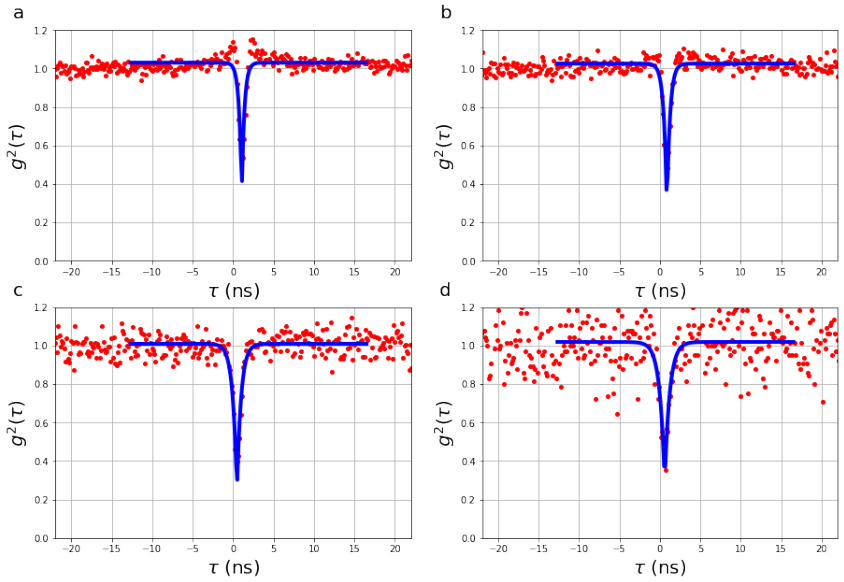

Figure 4.9 – Experimental second-order coherence measurements of cavity-quantum dot device 31.0-2.00. Blue curves represent a double exponential fit. **a-d** Second-order coherence $g^2(0) = 0.32$, $g^2(0) = 0.24$, $g^2(0) = 0.23$, and $g^2(0) = 0.27$ respectively. Excitation power before objective given by 39.8 ± 3.5 nW, 9.3 ± 0.8 nW, 4.6 ± 0.41 nW, and 1.15 ± 0.1 nW, respectively.

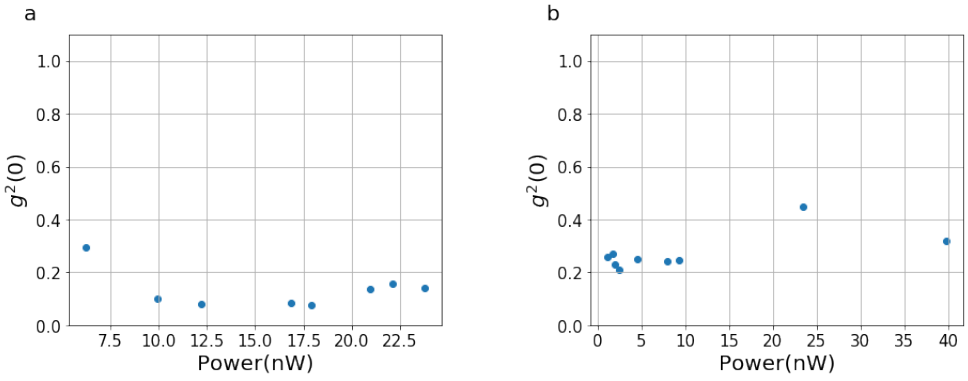

Figure 4.10 – Second-order coherence for different excitation powers. **a** 30.0-2.75, all measurements took 200 seconds **b** 31.0-2.00, all measurements took 100 seconds. Remark that the first data point in **a** shows a larger $g^2(0)$ caused by the very low count rate and that the measurement in **b** at 23.5 nW was measured with a larger cavity background.

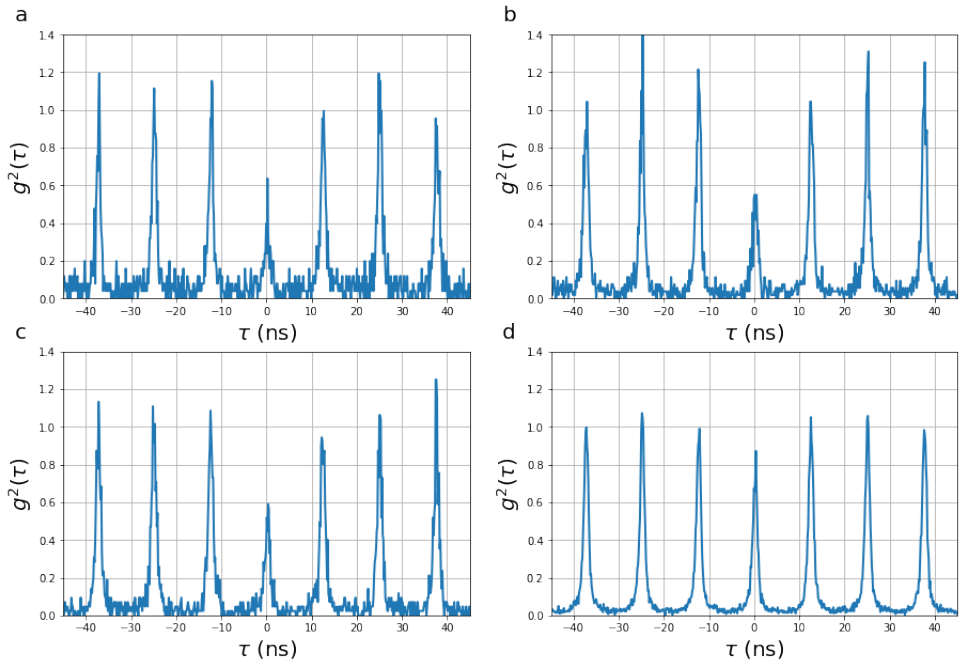

Figure 4.11 – Experimental second-order coherence measurement under excitation of a 80 MHz pulsed laser. Device 31.0-2.00 with an applied bias of 1.055 Volt. All measurements took 200 seconds. **a-d** laser power before objective respectively 0.88 ± 0.18 nW, 2.65 ± 0.18 nW, 3.36 ± 0.18 nW, and 8.0 ± 0.4 nW. Second-order correlations $g^2[0] = 0.32$, $g^2[0] = 0.50$, $g^2[0] = 0.56$, and $g^2[0] = 0.86$ respectively.

4.4.4 Second-order coherence of a split system

As explained in chapter 3, the quantum dot system has two eigenpolarisations. A question which can be asked is if it matters with what polarisation the quantum dot is excited for the purity of the single photons. In figure 4.12a two excited states of a quantum dot are observed; two roughly equal peaks show up at 0.998 Volt. The second-order coherence of both peaks has been measured from which can be concluded that both eigenpolarisations of this quantum dot show the same single-photon purity. This little experiment shows that it is apparently not important which mode is excited. However, when $g^2(0)$ was measured for a frequency between the two quantum dot modes no bunching or anti-bunching behaviour was observed.

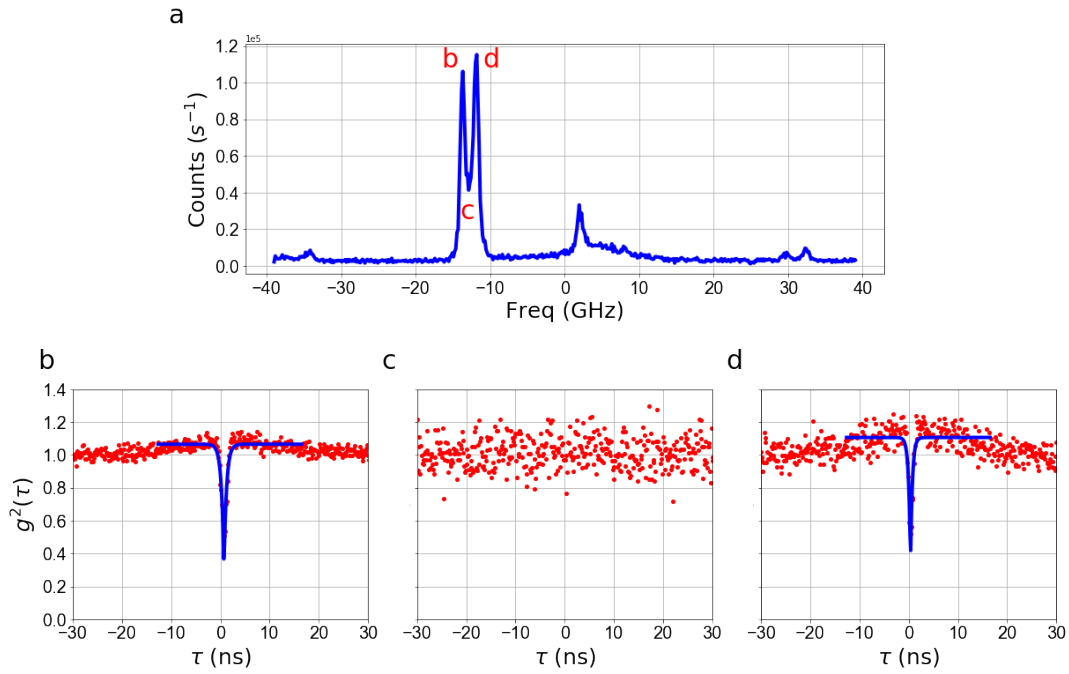

Figure 4.12 – A split system in device 30.5-2.75. **a** Photon count/s at 0.998 Volt **b-d** Second-order coherence at left peak, between two peaks and at right peak. $g^2(0) = 0.24$, $g^2(0) = 1$ and $g^2(0) = 0.23$, respectively.

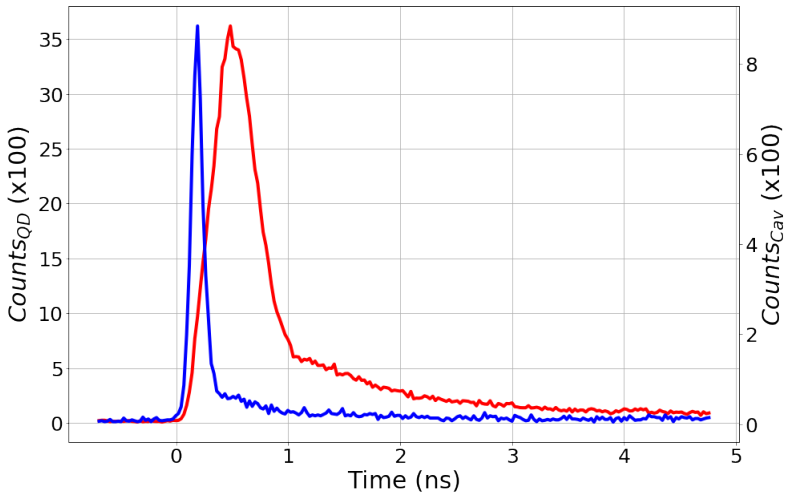

Figure 4.13 – Photon count versus time. Red curve indicates photon count versus time for device 31.0-2.00 with a quantum dot i.e. an applied bias of 1.055 Volt. Blue curve indicates the counts coming from an empty cavity i.e. for an applied bias of 0.655 Volt. Both curves were measured in cross polarisation for 100 seconds with a measured power of 11.5 ± 1.1 nW before the objective. Both measured using the ID Quantique photon detectors.

4.5 Lifetime of the quantum dot

The lifetime of the quantum dot is measured using the earlier introduced Hanbury Brown and Twiss setup, with one detector connected directly to the 12.5 ns period pulsed laser instead of one of the beamsplitter arms. The start/stop circuit board is connected to the cross polarised signal emitted from the cavity-quantum dot system and to the pulsed laser. The signal from the pulsed laser is used as the start of the detection. To obtain this curve the Time Correlated Single Photon Counting technique is used. In figure 4.13 the photon count versus time is shown for the quantum dot in device 31.0-2.00. An exponential fit was made using Origin giving a lifetime of 290 ± 2.3 ps.

4.6 Conclusion

In section 4.2 a lot of quantum dots were observed in our samples, showing that the used growth process creates many quantum dots with roughly the same resonant frequency. Furthermore, the data showed that the samples act as good cavities with a high Purcell enhancement. Using the semi-

classical model the quantum dot and cavity properties were obtained in section 4.3. Also, these polarisation scans showed the diversity between samples in the size of the polarisation non-degeneracy. Finally, in section 4.4 the purity of the single photon sources were studied showing that a quantum dot in device 31.0-2.00 acts as a high-purity single photon source which can be used to possibly measure Rabi oscillations. Moreover, a short detour was made in section 4.5 to show the lifetime and decay of the quantum dot w.r.t. that of the cavity.

Chapter 5

Polarisation-resolved quantum dot emission

In this chapter it will be shown mathematically why it is possible to extinguish the cavity mode. Furthermore, a computer-controlled method coined *runMinimize* is introduced to extinguish the cavity mode. An argument for the proposed method is given and the obtained measurements are compared to the manual approach.

5.1 Motivation

In order to measure photon correlations, the second-order correlation of the emitted light or Rabi oscillations, our signal has to consist solely from quantum dot emission. Therefore, the light from the cavity has to be blocked. As explained in chapter 4 short laser pulses are required to measure Rabi oscillations in our system. Unfortunately, a simple Fourier transform tells us that a short pulse duration also means that this pulse will excite a broad range of frequencies. A full width at half maximum (FWHM) of 50 picoseconds correspondents to a broad excitation in frequency-space with a FWHM of 3.2 GHz. This broad excitation pulse causes a larger fraction of the light to be composed of cavity light, a small improvement in the way we block the cavity mode can thus improve our measurements substantially.

Version of July 16, 2018– Created July 16, 2018 - 17:34

5.2 Removal of excitation laser light

Remark that the eigenpolarisations of the quantum dot and the cavity do not overlap [table 4.1]. The quantum dot modes are given in the cavity basis as [eq. 3.4]:

$$\begin{aligned} |X\rangle &= \cos\theta_{qd}\,|H\rangle - \sin\theta_{qd}\,|V\rangle \\ |Y\rangle &= \sin\theta_{qd}\,|H\rangle + \cos\theta_{qd}\,|V\rangle \end{aligned} \tag{5.1}$$

Because a large fraction of the light does not interact with a quantum dot the state of the light leaving the cavity after excitation with a horizontally polarised wave is given by:

$$\begin{aligned} |S\rangle &= \sqrt{1-P_i}\,|H\rangle_{cav} + \sqrt{P_i}\,|H\rangle_{qd} \\ |S\rangle &= \sqrt{1-P_i}\,|H\rangle + \sqrt{P_i}\left(\cos\theta_{qd}\,|X\rangle + \sin\theta_{qd}\,|Y\rangle\right), \end{aligned} \tag{5.2}$$

where P_i is the probability that the coherent light source interacts with the quantum dot. Although initially, both light sources are in the $|H\rangle$ state, the light originating from the quantum dot evolves such that it can be written as a superposition of $|V\rangle$ and $|H\rangle$. Every round trip the light detunes from the horizontal incoming polarisation with a certain phase, different for the horizontal polarisation and vertical polarisation. Therefore, the two eigenpolarisations of the quantum dot acquire a phase difference ϕ [29, 33].

$$|S\rangle = \sqrt{1-P_i}\,|H\rangle_{cav} + \sqrt{P_i}\left(\cos\theta_{qd}\,|X\rangle + e^{-i\phi}\sin\theta_{qd}\,|Y\rangle\right) \tag{5.3}$$

By placing a polariser in front of the cavity the horizontally polarised light can be extinguished and only light from the quantum dot will be measured. Mathematically, a vertical polariser can be seen as a projection on the vertical axis. Ergo the detected signal $|S_{det}\rangle$ is given by:

$$|S_{det}\rangle = \langle V|S\rangle = (e^{-i\phi}-1)\sqrt{P_i}\cos\theta_{qd}\sin\theta_{qd}\,|V\rangle \tag{5.4}$$

This means that the detected signal will consist solely of single photons emitted by the quantum dot:

$$\|S_{det}\|^2 = \frac{1}{2}P_i\cos\phi\sin^2 2\theta_{qd} \tag{5.5}$$

This means that by placing a polariser after the sample the cavity light can be fully extinguished.

Version of July 16, 2018– Created July 16, 2018 - 17:34

5.3 Method behind *runMinimize*

The original setup was extended, not only with a polariser, but also with a few wave plates. Using a half wave plate, a quarter wave plate, and a polariser the cavity light can be removed. Rotating the phase retarders instead of the polariser has the additional benefit that it does not change the direction of the light beam in contrast to the polariser, such that the coupling to the fiber does not deteriorate. The four wave plates are put into computer controlled rotation stages, which can be controlled with the use of an universal motion controller. The cavity light is then blocked using *runMinimize*.

runMinimize works by measuring and analysing the photon count over a certain frequency range for an angle interval around the current angle of one wave plate. A full 360°-turn around the current angle will gives us a sinusoidal trace ergo a small deviation from the current angle can be approximated by a second-order polynomial. Thus, a second-order polynomial is fitted through the measured data and the wave plate in question will be moved to this fitted deviation from the current value. This can be done successively for all four wave plates.

This sequential method can be justified by looking at the underlying mathematics. The effect of a wave plate on the polarisation of a beam can be described with the use of Jones calculus [34]. In Jones calculus the polarisation of a wave is given by a two-dimensional vector, while the optical elements and samples can be written as matrices. For example a quarter wave plate and a linear polariser can be represented, respectively, as:

$$A_{qwp} = e^{i\pi/4}\begin{pmatrix} 1 & 0 \\ 0 & i \end{pmatrix} \quad , \quad A_{pol} = \begin{pmatrix} 1 & 0 \\ 0 & 0 \end{pmatrix} \tag{5.6}$$

A rotated wave plate can be described as a multiplication of the above matrices times a rotation matrix. It is thus clear from the multiplication of different Jones matrices that the minimum angle of one operator is independent of the angle of other operators, as long as we are close to a (local) minimum. A toy-system with a quarter wave plate and a polarizer with angles with respect to the horizontal axis given by ϕ and θ generates a final state given by:

$$\vec{\mathbf{E}}_{\mathbf{f}} = R(\theta)A_{pol}R(\theta)^{-1}R(\phi)A_{qwp}R(\phi)^{-1}\vec{\mathbf{E}}_{\mathbf{i}}, \tag{5.7}$$

where $R(\phi)$ and $R(\theta)$ are the rotation matrices for the angle with respect to the horizontal axis for the quarter wave plate and the polariser respec-

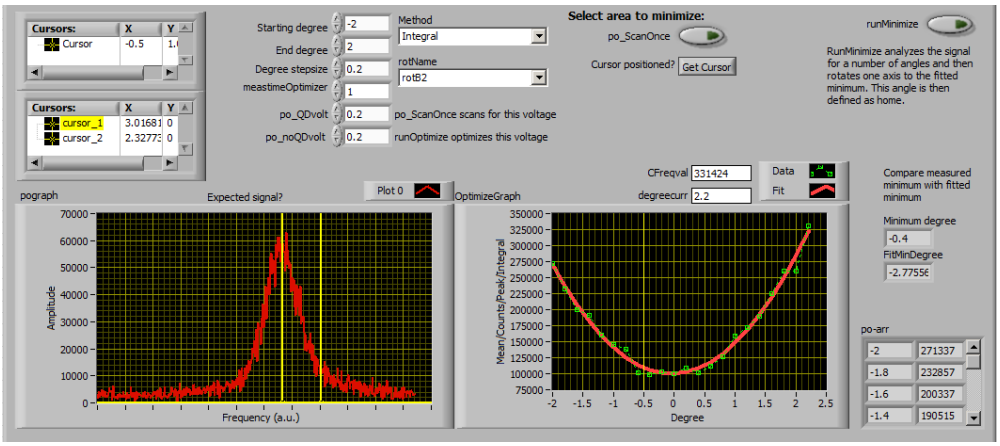

Figure 5.1 – The graphical user interface of *runMinimize*. The graph left shows the current signal, with the yellow lines enclosing the area of interest. The right graph shows the analysed data of the signal for different angles and the fitted line.

tively. Minimising the intensity is thus equal to finding those angles where the following holds:

$$\frac{\partial}{\partial\phi}\frac{\partial}{\partial\theta}\left\|\vec{\mathbf{E}}_\mathbf{f}\right\|^2 = 0 \tag{5.8}$$

$$\frac{\partial^2}{\partial\phi^2}\frac{\partial^2}{\partial\theta^2}\left\|\vec{\mathbf{E}}_\mathbf{f}\right\|^2 > 0 \tag{5.9}$$

$$\left\|\vec{\mathbf{E}}_\mathbf{f}\right\|^2_{\theta\theta}\left\|\vec{\mathbf{E}}_\mathbf{f}\right\|^2_{\phi\phi} - \left(\left\|\vec{\mathbf{E}}_\mathbf{f}\right\|^2_{\theta\phi}\right)^2 > 0 \tag{5.10}$$

Schwarz's theorem states that for continuous derivatives the order in which the derivatives are done is not important. Thus it is possible to first minimise the function with respect to θ and then minimise this function with respect to ϕ. Thus the method used in *runMinimize* is valid.

Four different analysis methods are implemented. Three of those minimise the counts in a certain frequency range. We found that the method most suitable for creating a cross-polarisation condition is an integral over the photon count in the selected frequency range. Obviously, this involves a step in which the frequency of the laser is varied and the photon count is measured for the frequencies in the frequency range.

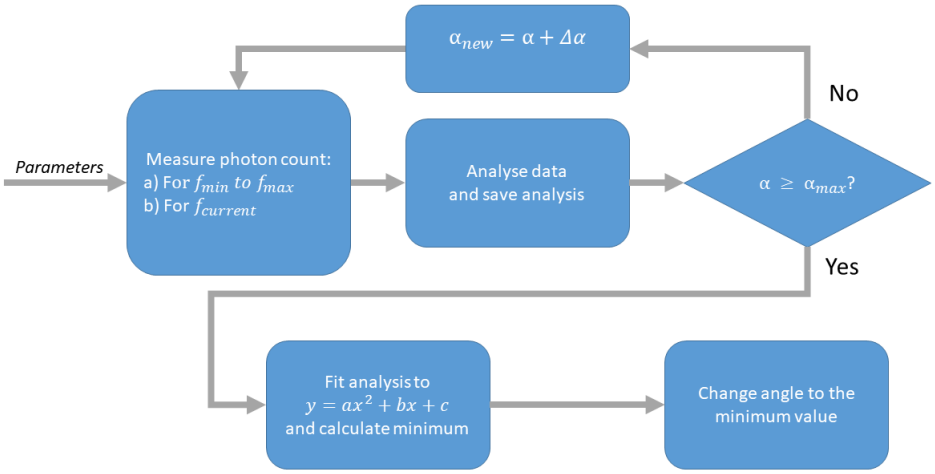

Figure 5.2 – Block diagram of *runMinimize*. User selected parameters include the integration time Δt, the degree step $\Delta\alpha$, the angle range $[\alpha_{min}, \alpha_{max}]$, the wave plate, the analysis method, and using two cursors, a frequency domain $[f_{min}, f_{max}]$. Block 1 measures the photon count for $[f_{min}, f_{max}]$ for three possible methods (integration, mean photon count, peak height) and measures the photon count for the current laser frequency for the single frequency method.

For experiments that are measured at a single frequency, such as second-order coherence measurements, another method is implemented. This method minimises the signal for a single frequency. Because the current experimental setup cannot tune the laser to the exact previous frequency, a scan over a frequency range would change the frequency of the laser and be extremely unhelpful. For the excitation with a pulsed laser, for which the frequency is not easily varied, the single frequency optimisation is also used.

5.4 Demonstration of *runMinimize*

In figure 5.3 the effect of the optimisation on the detected signal is seen. It is visible that the program optimises the signal and steadily moves towards a (local) minimum. We also observe that it is needed to minimise the signal with respect to a certain wave plate at least twice to find an optimal situation. This is partly due to the fitting procedure that is used in this program. It fits the analysed data through the measured angles and returns fitted values only for the measured angles. If the actual minimum

is placed between two data points, the angle of the wave plate is set to the angle corresponding to the closest data point.

A clear comparison between the results obtained with manual optimisation and computer-controlled optimisation can be seen in figure 5.4. Four voltage scans are shown in cross polarisation condition. Figure 5.4b shows that the same results **can** be obtained using manual optimisation. However, if all measurements are taken into account we observe that *runMinimize* is able to return the same extinguishment for multiple systems. A second advantage, not shown in the figures, is that this method is a lot faster than manual optimisation.

The most important advantage of this method over manual optimisation is that it is possible to extinguish the cavity for just some frequencies. In figure 5.5 the signal was minimised around the resonant frequency of a certain quantum dot of device 31.0-2.00. It is clear that the program works as expected and minimises the signal given the constraints. The program could be improved by using a Gaussian window instead of a rectangular window for the integration. This change gives more weight to the centre of the frequency domain, effectively giving more weight to noise reduction at the quantum dot frequency. Another improvement that could be implemented is changing the fitting procedure such that it can also return angles between measured angles.

Version of July 16, 2018– Created July 16, 2018 - 17:34

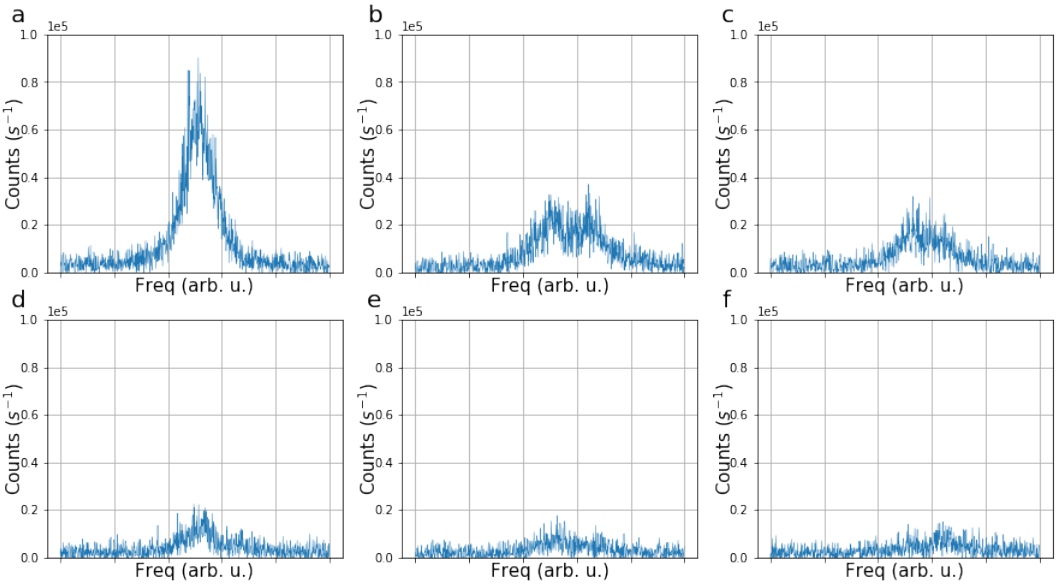

Figure 5.3 – Transmitted photon counts/s without a quantum dot. The photon count after manual optimisation (**a**), optimisation of HWP before objective (**b**), the QWP before objective (**c**), QWP after objective (**d**), HWP after objective (**e**), and again HWP before the objective (**f**).

Version of July 16, 2018– Created July 16, 2018 - 17:34

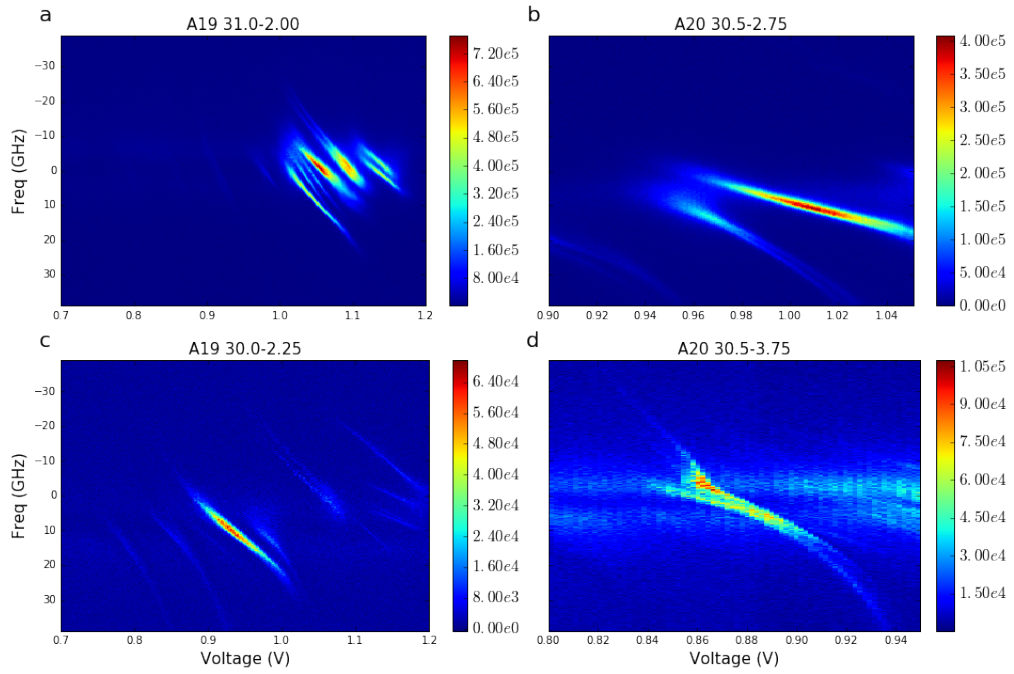

Figure 5.4 – Colours plots show $I(f, V)$ in crosspolarisation for four different cavity-quantum dot devices . Figures **a** and **c** are obtained with the use of *run-Minimize*, while figures **b** and **d** are obtained by turning the polariser by hand.

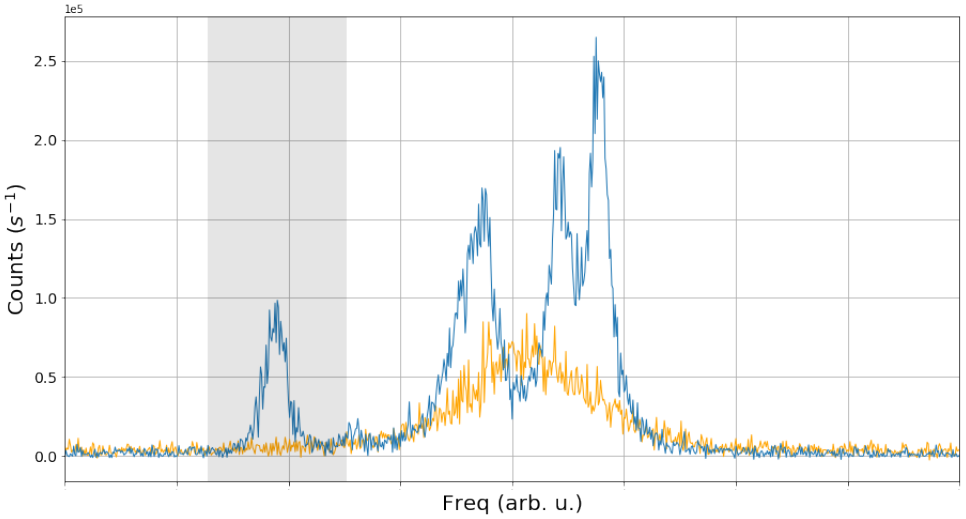

Figure 5.5 – Transmitted photon count/s of a cavity-quantum dot system. The grey rectangle indicates (roughly) the frequency range that was extinguished, the blue curve and orange curves show the count at 1.055 Volt and 0.655 Volt respectively. The sharp peaks in the blue curve are quantum dots.

Version of July 16, 2018– Created July 16, 2018 - 17:34

Chapter 6

Experimental observations of Rabi oscillations in a cavity-quantum dot system

A general scheme to indirectly measure Rabi oscillations in polarisation non-degenerate cavity-quantum dot systems was given in the introduction as:

1. Find an efficient and reliable single-photon source;
2. Reduce light from other light sources;
3. Measure the number of photons emitted from this source as a function of laser power.

Recall that we have shown in chapter **4** that device 31.0-2.00 acts as an efficient and reliable single-photon source. Also, the demonstration of *runMinimize* in chapter **5** showed how well the cavity could be extinguished for this device. This chapter will discuss the third point in more detail. First, the methodology to measure Rabi oscillations will be discussed in more detail. The latter sections will discuss the results obtained and study the effects of the detuning Δ between the mean cavity frequency and the quantum dot frequency on the observation of Rabi oscillations.

Version of July 16, 2018– Created July 16, 2018 - 17:34

6.1 Methodology

Rabi oscillations are indirectly measured by measuring the emitted photon count versus the pump power of the pulsed laser. During a laser pulse a non-zero intensity is present and the state of the exciton oscillates between the ground and the excited state as explained in chapter 2. After the (short) laser pulse, the electric field is zero and no Rabi oscillations take place anymore. Thus **Rabi oscillations happen during a pulse**. The exciton then possibly decays to the ground state via spontaneous emission. A pulse with a different pulse area drives the exciton to a different end state and thus results in a different photon count ($I \propto P_e$, the excited state probability amplitude). In this view we neglect emission during a pulse, because our pulses are relatively short. This method was also used by Giesz et al. [22]. A schematic view of this method is shown in figure 6.1.

Furthermore, to remove cavity light leaked through the polariser the photon count without a quantum dot is subtracted from the photon count with a quantum dot. The measurements showing quantum dot emission w.r.t. the pump power in this chapter show $N_y = S_{qd} - S_{cav}$. Here N_y is the photon count of the quantum dot, S_{qd} the photon count with a quantum dot and S_{cav} the photon count without a quantum dot

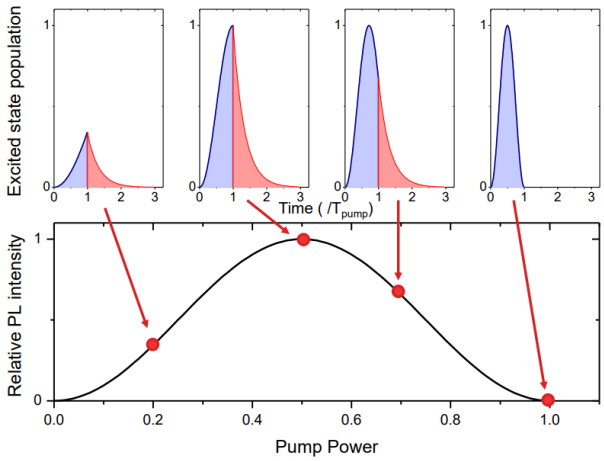

Figure 6.1 – Schematic of the used method. The top row shows the excited state population for increasing pulsed laser powers. Blue shows the excited state population during a pulse versus time, while red shows the decay to the ground state via spontaneous emission. Arrows show the corresponding data point in a Rabi measurement. Figure taken from [22].

Version of July 16, 2018– Created July 16, 2018 - 17:34

6.2 Experimental observation

In figure 6.2a the photon count of the quantum dot is plotted against the square root of the photon count from the laser for a bias of 1.055 Volt. Because $I \propto E^2$ and $I \propto N$ the square root of the laser counts is proportional to the electric field. A few observations should be made about this measurement:

1. Clear oscillations in the luminosity are seen;
2. $Counts_{qd}$ increases indefinitely.

The first observation suggests that in fact Rabi oscillations were measured in the cavity-quantum dot samples. The second observation is however quite unexpected. In figure 6.3 three different possible contributions are fitted to the data: square root contribution, linear contribution, and a saturation curve contribution. Remark that all these fits use a simple, but incomplete, function to describe the decay of the oscillations. As shortly mentioned in chapter 2 the probability amplitude of the excited state decays w.r.t. time to a certain asymptotic value. Considering that the system is, however, constantly excited with short (50 ps) pulses, the decay of the Rabi oscillations is expected to be the same for higher powers i.e. the amplitude of the oscillations should not decay for larger powers.

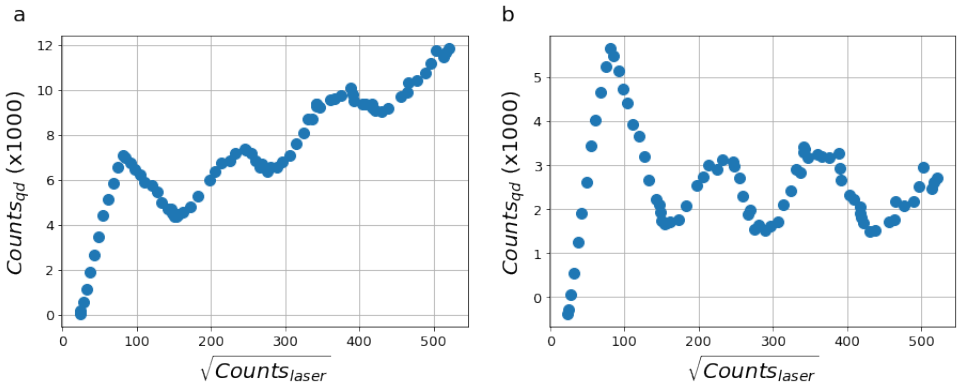

Figure 6.2 – **a** Experimental resonant excitation photon count signal for the quantum dot in device 31.0-2.00 with an applied bias of 1.055 Volt. **b** A square root contribution subtracted from figure 6.2a.

The data is fitted using a least squares optimisation algorithm with, in case of square root contribution, the following fit:

$$N_y = A \cdot e^{-\Gamma N_x} \sin^2\left(f \cdot \sqrt{N_x}\right) + B \cdot \sqrt{N_x}, \tag{6.1}$$

where N_y and N_x are the detected counts on the vertical axis and horizontal axis, respectively. A the amplitude of the sinusoidal function, Γ the decay rate, f the frequency, and B the amplitude of the unknown contribution. The saturation curve contribution is fitted with:

$$N_y = A \cdot e^{-\Gamma N_x} \sin^2\left(f \cdot \sqrt{N_x}\right) + \frac{A}{B + CN_x^{-1}}, \tag{6.2}$$

The added part simulates the saturation of the quantum dot by a continuous wave laser. If our laser emits pulsed light with a continuous wave background, a continuous wave saturation curve would contribute to our curve signal.

The fitting parameters and χ^2-values are found in table 6.1. Note that the saturation curve model has two more free parameters to fit the data to the model and thus can more easily achieve a lower χ^2-value. The data fitted to Rabi oscillations at 1.055 Volt and 1.015 Volt clearly suggests that there is a square root contribution to the signal. For all measurements, the lowest χ^2 value is obtained for the square root model. Furthermore, the obtained values are relatively close, while other models give vastly different values for different measurements. Also, the apparent trend is best continued by the square root contribution model. In figure 6.2b the measurement at 1.055 Volt is shown with a square root contribution subtracted.

However, why we observe a square root background remains an open question. A possible suggestion could be other light sources in the solid-state structure. An interesting parallel can be seen with the density of states for an unrestricted system (not confined in any spatial direction), which shows a square root behaviour with respect to the energy, resulting in square root behaviour in emission with respect to the photon count [26].

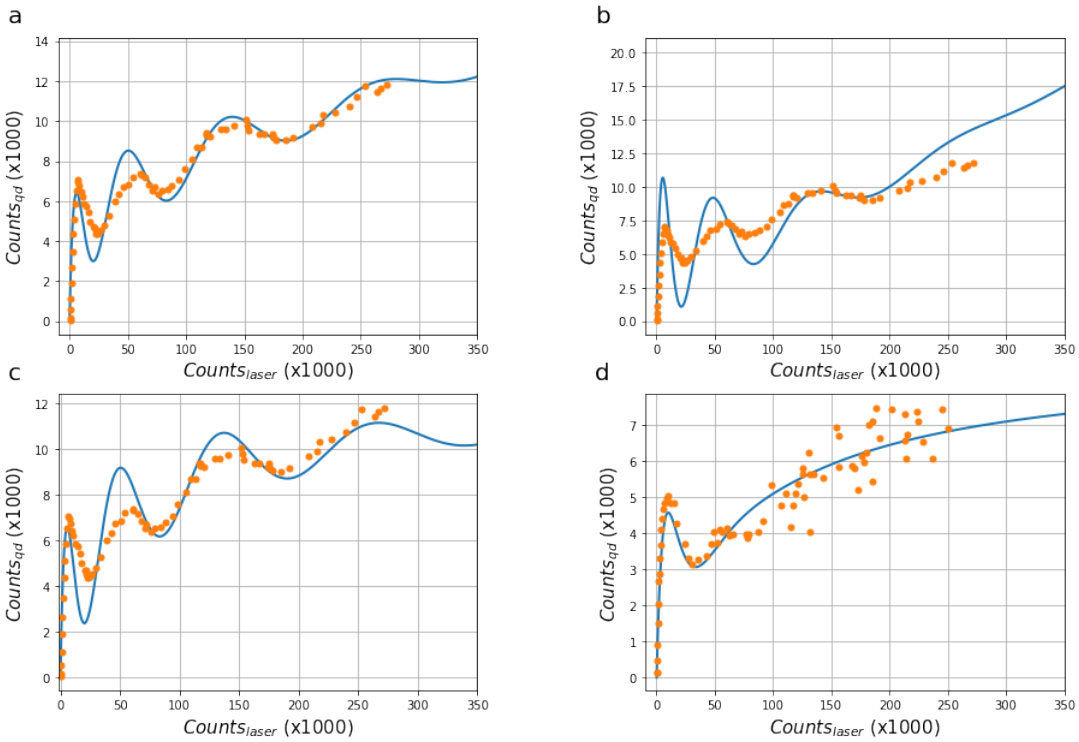

Figure 6.3 – Rabi oscillations fitted with three different models. **a** Square root background model (1.055 Volt) **b** Linear background model (1.055 Volt) **c** Saturation curve model (1.055 Volt) **d** Saturation curve model (1.015 Volt).

	Fig. 6.3a	**Fig. 6.3b**	**Fig. 6.3c**	**Fig. 6.3d**	**Fig. 6.4d**
Bias	1.055 Volt	1.055 Volt	1.055 Volt	1.015 Volt	1.015 Volt
Amplitude	$5.0 \cdot 10^3$	$1.1 \cdot 10^4$	$6.1 \cdot 10^3$	$6.0 \cdot 10^3$	$6.0 \cdot 10^3$
$\Gamma \quad (N^{-1})$	$4.9 \cdot 10^{-6}$	$1.0 \cdot 10^{-5}$	$5.0 \cdot 10^{-6}$	$5 \cdot 10^{-5}$	$5.0 \cdot 10^{-6}$
Freq. $(N^{-\frac{1}{2}})$	$2.1 \cdot 10^{-2}$	$2.1 \cdot 10^{-2}$	$2.1 \cdot 10^{-2}$	$1.4 \cdot 10^{-2}$	$1.4 \cdot 10^{-2}$
Sqrt. ampl.	20.65				14.9
Linear ampl.		$5.0 \cdot 10^{-2}$			
A			$8.9 \cdot 10^5$	$1.0 \cdot 10^7$	
B			69	$1.1 \cdot 10^3$	
C			$6.4 \cdot 10^6$	$8.7 \cdot 10^7$	
χ^2	12642	110932	26833	5451	5177

Table 6.1 – The parameters used to fit the Rabi oscillations at 1.055 Volt (**a-c**) and 1.015 Volt (**d** and **6.4d**) to a few models. Remark that the saturation model gives vastly different values for the same parameter at 1.055 Volt and 1.015 Volt.

6.3 Effect of the detuning on the observation of Rabi oscillations

In figure 6.4 the photon count of the quantum dot is plotted against the photon count from the laser for four different applied voltages. As could be seen in figure 4.2a this corresponds to a decreasing detuning between the cavity frequency and the quantum dot frequency. Remark that the laser is still resonant with the quantum dot. We observe that for a large $\Delta = |\omega_{cav} - \omega_{qd}|$ Rabi oscillations are more clearly observed. At a large detuning the Purcell enhancement and cooperativity decrease and thus the system enters the free-space regime, for which Rabi oscillations were more often observed [10, 17]. The data is fitted with the square root background model introduced in the last section. The fitting parameters can be found in table 6.2. Remark that the frequency is apparently not influenced by Δ and that the fitted frequencies have approximately the same value.

A possible explanation why Rabi oscillations are harder to observe in cavity-quantum dot systems might be that the increased decay rate due to the Purcell effect could cause the subsequent maxima to be a lot lower than in free-space quantum dot systems. Furthermore, a second explanation could be that the excitation of the quantum dot by a broad cavity peak also starts non-resonant Rabi oscillations with slightly different frequencies, which reduces the clarity of the oscillations.

Version of July 16, 2018– Created July 16, 2018 - 17:34

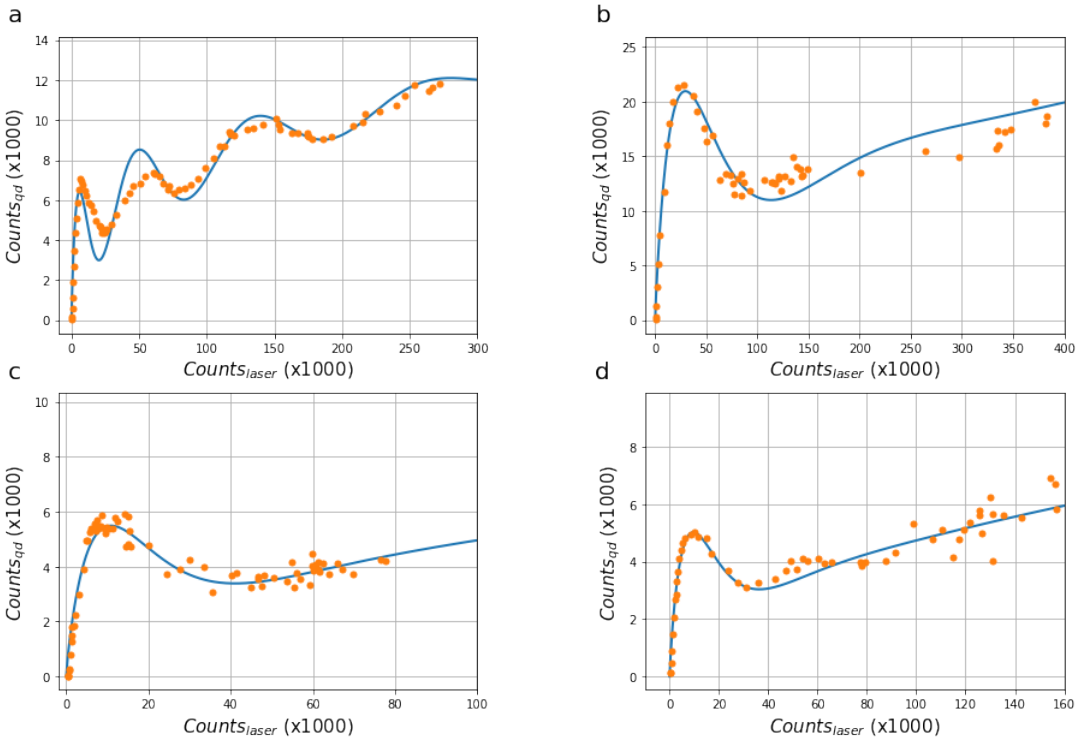

Figure 6.4 – Experimental resonant excitation photon count signal for a quantum dot on and off resonance with the cavity mode. **a** bias: 1.055V, **b** bias: 1.035V, **c** bias: 1.02V, **d** bias: 1.015V. Intensity measured by measuring the photon count at the given voltages and subtracting the counts at 0.655V. Power measured by shifting a half wave plate by 5 degrees and counting the photon count at 0.655V. Figures **a-d** range from far from cavity resonance to resonant with cavity. Blue curve shows the fit with square root contribution.

	Figure a	**Figure b**	**Figure c**	**Figure d**
Bias	1.055 Volt	1.035 Volt	1.020 Volt	1.015 Volt
Amplitude	$5.0 \cdot 10^3$	$2.2 \cdot 10^4$	$6.7 \cdot 10^3$	$6.0 \cdot 10^3$
$\Gamma \quad (N^{-1})$	$4.9 \cdot 10^{-6}$	$1.1 \cdot 10^{-5}$	$4.6 \cdot 10^{-6}$	$5.0 \cdot 10^{-6}$
Frequency $\quad (N^{-\frac{1}{2}})$	$2.1 \cdot 10^{-2}$	$8.5 \cdot 10^{-3}$	$1.3 \cdot 10^{-2}$	$1.4 \cdot 10^{-2}$
Square root amplitude	20.65	31.2	15.5	14.9
χ^2	12642	15943	6960	5177

Table 6.2 – The four parameters used to fit the intensity vs laser counts for the same quantum dot for four different detunings with respect to the cavity to a Rabi oscillations with square root background model.

Chapter 7

Conclusion and future outlook

In chapter 6 a demonstration of Rabi oscillations between the ground and excited state of a self-assembled quantum dot has been presented. This shows that the state of a quantum dot in a cavity can be controlled by a sequence of pulses. Potentially, these systems can be used for multiple applications. Furthermore, we have shown that Rabi oscillations can be more easily seen by tuning the quantum dot out of resonance with the cavity and thus decreasing the advantages of a cavity-quantum dot system. One glaring difference is seen with respect to our prediction; a square root contribution is observed in our measurements.

Also, an automation system has been introduced to do these types of measurements faster, more reproducible and with greater accuracy. Without this method, it would have been a lot harder to constantly obtain the level of extinguishment needed to observe Rabi oscillations in device 31.0-2.00.

Outlook

An interesting next step would be to look at the creation of multi-photon effects. As shown by Fischer et al. [20] self-assembled quantum dots in free-space exhibit two-photon emission under pulsed excitation which are out of phase with the Rabi oscillations. These effects could in theory be observed if the system is a high-purity single photon source under pulsed laser excitation at low powers. In other words, to measure these effects the system should show a second-order correlation of $g^2(0) < 1$ for low pulsed laser excitation. Furthermore, as shown in the master thesis of David Kok this does not necessarily mean that Rabi oscillations are visible. Thus, the second criteria is that the device should exhibit clear Rabi oscillations. Also, a better control on the pulse duration of the pulsed laser is required since multi-photon effects also depend heavily on the pulse duration. In theory, multi-photon effects can now be seen by measuring the second-order correlation for a range of excitation powers.

Unfortunately, the measurement of second-order correlations is a slow process. The measurement of one data point would take around 200 seconds, and at least 10 data points should be measured for a reliable result. Remark now that the Rabi oscillation measurements showed in chapter 6 took at most 450 seconds, already showing a very unstable system at the higher powers. Moreover, as Fischer showed the two-photon emission does not follow a simple sine wave with respect to the excitation power, but has sharp peaks and broader valleys. Altogether, this method requires a very stable system and can possibly not be measured in a automated way.

Chapter 8

Acknowledgement

During my time in the quantum optics group I met a lot of great people who helped me to grasp the physics behind my project and gave valuable insights in how to do research and who welcomed me with open arms. In particular I would like to thank Henk Snijders, my direct supervisor, who learned me the ropes of experimental physics and cavity quantum electrodynamics and who was always available to help. Of course, I also like to thank Wolfgang Löffler for his valuable insights and discussions. I would like to thank them for the opportunity to be able to work in a lab with almost no need to schedule lab time. Furthermore, a special thanks to Evert, Daan, Stefano, Snigdh, and Guido, all of whom I (temporarily) shared an office with, for the interesting discussions in both physics related as non-physics related subjects.

Bibliography

[1] D. Deutsch and R. Jozsa, *Rapid Solution of Problems by Quantum Computation*, Proceedings of the Royal Society A: Mathematical, Physical and Engineering Sciences **439**, 553 (1992).

[2] P. Shor and P. W., *Algorithms for quantum computation: discrete logarithms and factoring*, in *Proceedings 35th Annual Symposium on Foundations of Computer Science*, pages 124–134, IEEE Comput. Soc. Press, 1994.

[3] J. J. Pla, K. Y. Tan, J. P. Dehollain, W. H. Lim, J. J. L. Morton, D. N. Jamieson, A. S. Dzurak, and A. Morello, *A single-atom electron spin qubit in silicon*, Nature **489**, 541 (2012).

[4] M. Aspelmeyer, T. J. Kippenberg, and F. Marquardt, *Cavity optomechanics*, Reviews of Modern Physics **86**, 1391 (2014).

[5] L. M. K. Vandersypen and I. L. Chuang, *NMR techniques for quantum control and computation*, Reviews of Modern Physics **76**, 1037 (2005).

[6] T. Pittman, B. Jacobs, and J. Franson, *Quantum computing using linear optics*, Johns Hopkins Apl Technical Digest **25**, 84 (2004).

[7] P. Kok, W. J. Munro, K. Nemoto, T. C. Ralph, J. P. Dowling, and G. J. Milburn, *Linear optical quantum computing with photonic qubits*, Reviews of Modern Physics **79**, 135 (2007).

[8] Chen, Bonadeo, Steel, Gammon, Katzer, Park, and Sham, *Optically induced entanglement of excitons in a single quantum Dot*, Science (New York, N.Y.) **289**, 1906 (2000).

[9] P. Michler, A. Imamoglu, M. D. Mason, P. J. Carson, G. F. Strouse, and S. K. Buratto, *Quantum correlation among photons from a single quantum dot at room temperature*, Nature **406**, 968 (2000).

[10] T. H. Stievater, X. Li, D. G. Steel, D. Gammon, D. S. Katzer, D. Park, C. Piermarocchi, and L. J. Sham, *Rabi Oscillations of Excitons in Single Quantum Dots*, Physical Review Letters **87**, 133603 (2001).

[11] A. Reiserer and G. Rempe, *Cavity-based quantum networks with single atoms and optical photons*, Reviews of Modern Physics **87**, 1379 (2015).

[12] M. L. Bellac, *Quantum Physics*, Cambridge University Press, Cambridge, 2006.

[13] P. Knight and C. Gerry, *Introductory Quantum Optics*, Cambridge University Press, Cambridge, 2005.

[14] M. Fox, *Quantum Optics*, Oxford University Press, Oxford, 2006.

[15] M. P. Bakker, A. V. Barve, A. Zhan, L. A. Coldren, M. P. van Exter, and D. Bouwmeester, *Polarization degenerate micropillars fabricated by designing elliptical oxide apertures*, Applied Physics Letters **104**, 151109 (2014).

[16] J. Gudat, *Cavity Quantum Electrodynamics with Quantum Dots in Microcavities*, PhD thesis, Leiden University, 2012.

[17] A. Zrenner, E. Beham, S. Stufler, F. Findeis, M. Bichler, and G. Abstreiter, *Coherent properties of a two-level system based on a quantum-dot photodiode*, Nature **418**, 612 (2002).

[18] E. B. Flagg, A. Muller, J. W. Robertson, S. Founta, D. G. Deppe, M. Xiao, W. Ma, G. J. Salamo, and C. K. Shih, *Resonantly driven coherent oscillations in a solid-state quantum emitter*, Nature Physics (2009).

[19] V. Giesz, N. Somaschi, G. Hornecker, T. Grange, B. Reznychenko, L. De Santis, J. Demory, C. Gomez, I. Sagnes, A. Lematre, O. Krebs, N. D. Lanzillotti-Kimura, L. Lanco, A. Auffeves, and P. Senellart, *Coherent manipulation of a solid-state artificial atom with few photons*, Nature Communications **7** (2016).

[20] K. A. Fischer, L. Hanschke, J. Wierzbowski, T. Simmet, C. Dory, J. J. Finley, J. Vučković, and K. Müller, *Signatures of two-photon pulses from a quantum two-level system*, Nature Physics **13**, 649 (2017).

[21] K. A. Fischer, K. Müller, K. G. Lagoudakis, L. Hanschke, M. Kremser, J. J. Finley, and J. Vučković, *Dynamical modeling of pulsed two-photon interference Pulsed Rabi oscillations in quantum two-level systems: beyond the area theorem*, Quantum Sci. Technol **3** (2018).

[22] V. Giesz, *Cavity-enhanced Photon-Photon Interactions With Bright Quantum Dot Sources*, PhD thesis, Université Paris-Saclay, 2015.

[23] E. Flagg, *Coherent control and decoherence of single semiconductor quantum dots in a microcavity*, PhD thesis, University of Texas, 2008.

[24] M. P. Bakker, A. V. Barve, T. Ruytenberg, W. Löffler, L. A. Coldren, D. Bouwmeester, and M. P. van Exter, *Polarization degenerate solid-state cavity quantum electrodynamics*, Phys. Rev. B **91**, 115319 (2015).

[25] S. H. Simon, *The Oxford solid state basics*, Oxford Univ. Press, Oxford, UK, 2013.

[26] C. Kittel, *Introduction to Solid State Physics*, John Wiley, New York, 6 edition, 1986.

[27] B. E. A. Saleh and M. C. Teich, *Fundamentals of photonics*, Wiley-Interscience, 2007.

[28] D. A. B. Miller, D. S. Chemla, T. C. Damen, A. C. Gossard, W. Wiegmann, T. H. Wood, and C. A. Burrus, *Band-Edge Electroabsorption in Quantum Well Structures: The Quantum-Confined Stark Effect*, Physical Review Letters **53**, 2173 (1984).

[29] D. Kok, *Single photons and coherent light in polarized quantum dot cavity QED*, Master's thesis, 2017.

[30] M. P. Bakker, T. Ruytenberg, W. Löffler, A. Barve, L. Coldren, M. P. van Exter, and D. Bouwmeester, *Quantum dot nonlinearity through cavity-enhanced feedback with a charge memory*, Phys. Rev. B **91**, 241305 (2015).

[31] K. L. Silverman, R. P. Mirin, S. T. Cundiff, and A. G. Norman, *Direct measurement of polarization resolved transition dipole moment in InGaAs/GaAs quantum dots*, Applied Physics Letters **82**, 4552 (2003).

[32] P. G. Eliseev, H. Li, A. Stintz, G. T. Liu, T. C. Newell, K. J. Malloy, and L. F. Lester, *Transition dipole moment of InAs/InGaAs quantum dots from experiments on ultralow-threshold laser diodes*, Applied Physics Letters **77**, 262 (2000).

[33] M. van de Stolpe, *Optimizing the polarization for a brighter CQED Single Photon Source*, Master's thesis, 2017.

[34] E. Collet, *Field Guide to Polarization*, SPIE, 2005.

Version of July 16, 2018– Created July 16, 2018 - 17:34